CHALMERS
UNIVERSITY OF TECHNOLOGY

Effects of riverbank erosion on the stability of surrounding infrastructure

A case study of the Nolhaga wastewater treatment plant

Master's thesis in Infrastructure and Environmental Engineering

EMIL THEODORSSON

DEPARTMENT OF ARCHITECTURE AND CIVIL ENGINEERING

CHALMERS UNIVERSITY OF TECHNOLOGY
Gothenburg, Sweden 2024
www.chalmers.se

Master's thesis 2024

Effects of riverbank erosion on the stability of surrounding infrastructure

A case study of the Nolhaga wastewater treatment plant

EMIL THEODORSSON

CHALMERS
UNIVERSITY OF TECHNOLOGY

Department of Architecture and Civil Engineering
Division of Geology and Geotechnics
Chalmers University of Technology
Gothenburg, Sweden 2024

Effects of riverbank erosion on the stability of surrounding infrastructure
A case study of the Nolhaga wastewater treatment plant
EMIL THEODORSSON

Supervisor: Amardeep Amavasai, Ramboll
Supervisor: Tara Wood, Ramboll
Examiner: Minna Karstunen, Department of Architecture and Civil Engineering

Master's Thesis 2024
Department of Architecture and Civil Engineering
Division of Geology and Geotechnics
Chalmers University of Technology
SE-412 96 Gothenburg
Telephone +46 31 772 1000

Cover: Aerial photo over the Nolhaga wastewater treatment plant (© Lantmäteriet).

Typeset in LaTeX
Printed by Chalmers Reproservice
Gothenburg, Sweden 2024

Effects of riverbank erosion on the stability of surrounding infrastructure
A case study of the Nolhaga wastewater treatment plant
EMIL THEODORSSON
Department of Architecture and Civil Engineering
Chalmers University of Technology

Abstract

The impacts of climate change, such as more frequent and severe rainfall and longer periods of drought, may heighten the likelihood and regularity of erosion along riverbanks. This could result in negative outcomes for both ecosystems and human activities in the vicinity. Most studies that analyse the effects of bank erosion do not account for the influence of soil properties such as anisotropy or creep. They also rarely investigate how surrounding structures are affected by the erosion process. This thesis aims to use the data collected from the Nolhaga wastewater treatment plant in Alingsås as a case study to assess these aspects. Regarding soil constitutive models, a comparison between the use of simple to more complex models have been considered in this thesis. The constitutive models considered include Mohr-Coulomb, Soft Soil Creep, and Creep-SCLAY1S. The Nolhaga test site is modelled in *PLAXIS 2D* finite element code as several 2D plane strain sections, using site investigation data as a source to model the geometry and soil properties. A total of five sections are modeled, the locations of which are based on a previously performed stability analysis. The assumed bank erosion rate and patterns are simplified to be equal across all five modeled sections, as well as evenly distributed over the entire riverbed that is below water. The majority of the loads considered in the sections are based on previous stability analyses. However, some have updated values from more recent load estimations. The results show that Creep-SCLAY1S generally predicts the highest vertical and horizontal displacements in the modeled sections, with Soft Soil Creep predicting the second highest vertical displacements, and Mohr-Coulomb predicting the second highest horizontal ones. The calculated safety factors of the riverbanks decrease with time as a direct result of modelling erosion, with some areas dropping below a safety factor of 1 within the studied time frame, indicating a risk of failure. Based on a displacement comparison with a non-erosion scenario, bank erosion has a large impact on predicted horizontal displacements, while having significantly less impact on the vertical ones. Based on a performed pipe tolerance assessment, the treatment plant pipelines are deemed to be at risk of suffering damage by the calculated displacements, with the influence of erosion on these risks being negligible. However, due to lack of relevant site data, there are large uncertainties related to these results. Thus, further investigations are recommended to gather more information and decrease these uncertainties.

Keywords: Riverbank erosion, finite element analysis, PLAXIS 2D, Mohr-Coulomb, Soft Soil Creep, Creep-SCLAY1S.

Acknowledgements

First and foremost, I would like to thank my supervisor, Dr Amardeep Amavasai, for always making time for me when I needed his guidance and support. His genuine and passionate interest in his work has inspired me, and given me a new perspective on what it means to be an engineer.

Secondly, I would like to thank my supervisor, Dr Tara Wood, and my examiner, Prof. Minna Karstunen, for assisting me with meaningful advice and direction throughout my entire thesis work.

Thirdly, I would like to thank Ramboll, for giving me the opportunity to write my thesis for them, and for providing me with the data that was necessary to be able to carry out my work.

I also would like to thank my coworkers at Ramboll, who have assisted me and given me important insights into the case study project, as well as into what it is like working in the industry.

Last but not least, I would like to thank my family and friends who, through their love and support, have gotten me through this incredibly challenging time. Without them it would simply not have been possible.

Emil Theodorsson, Gothenburg, June 2024

List of Acronyms

Below is the list of acronyms that have been used throughout this thesis listed in alphabetical order:

AC	after construction
CSS	current stress surface
FE	finite element
IC	initial conditions
ICS	Intrinsic Compression Surface
MC	Mohr-Coulomb
MCC	Modified Cam Clay
NCS	Normal Compression Surface
OCR	overconsolidation ratio
POP	pre-overburden pressure
SGI	Swedish Geotechnical Institute
SS	Soft Soil
SSC	Soft Soil Creep

Nomenclature

Below is the nomenclature of the Roman and Greek symbols that have been used throughout this thesis.

Roman symbols

c'	effective cohesion	[kPa]
c_{inc}	increase in effective cohesion with depth	[kPa/m]
c'_{ref}	reference effective cohesion	[kPa]
$c_{ref,inter}$	reference interface cohesion	[kPa]
D	pipe diameter	[mm]
E'	effective Young's modulus	[kPa]
E'_{ref}	reference effective Young's modulus	[kPa]
E^{ref}_{oed}	reference tangential oedometer modulus	[kPa]
e_0	initial void ratio	[-]
G'	effective shear modulus	[kPa]
K'	effective bulk modulus	[kPa]
K_0	lateral earth pressure at rest	[kPa]
K_0^{NC}	lateral earth pressure at rest for normally consolidated state	[kPa]
k	permeability	[m/s]
$M(\theta)$	stress ratio at critical state for Creep-SCLAY1S model	[-]
M^*	stress ratio at critical state for Soft Soil Creep model	[-]
M_c	stress ratio at critical state in triaxial compression	[-]
M_e	stress ratio at critical state in triaxial extension	[-]
M_{MC}	slope of Mohr-Coulomb failure line	[-]
p'	mean effective stress	[kPa]
p'_{eq}	effective equivalent mean stress	[kPa]

p'_i	intrinsic isotropic preconsolidation pressure	[kPa]
p'_p	isotropic preconsolidation pressure	[kPa]
q	deviatoric stress	[kPa]
S_t	sensitivity factor	[-]

Greek symbols

α	scalar inclination of yield surface	[-]
α_0	initial inclination of yield surface	[-]
α_{K0}	scalar inclination of yield surface in normally consolidated K_0 state	[-]
γ_{sat}	saturated unit weight	$[kN/m^3]$
γ_{unsat}	unsaturated unit weight	$[kN/m^3]$
ε_v	volumetric strain	[-]
ε_v^e	volumetric elastic strain	[-]
ε_v^c	volumetric creep strain	[-]
ε_q	deviatoric strain	[-]
ε_q^e	deviatoric elastic strain	[-]
ε_q^c	deviatoric creep strain	[-]
ζ	absolute rate of destructuration	[-]
ζ_d	relative rate of destructuration	[-]
η	stress ratio	[-]
η_{K0}	stress ratio in normally consolidated K_0 state	[-]
θ	lode angle	[-]
κ^*	modified swelling index	[-]
Λ	viscoplastic multiplier	[-]
λ^*	modified compression index	[-]
λ_i^*	modified intrinsic compression index	[-]
μ^*	modified creep index	[-]
μ_i^*	modified intrinsic creep index	[-]
ν'	Poisson's ratio	[-]
ν'_{ur}	Poisson's ratio for unloading-reloading	[-]
σ'_1	vertical effective stress in principal stress space	[kPa]
σ'_3	horizontal effective stress in principal stress space	[kPa]

$\vec{\sigma}_d$	deviatoric stress vector	[-]
τ	reference time	[days]
φ'	friction angle	[°]
φ'_{cv}	critical state friction angle	[°]
φ_{inter}	interface friction angle	[°]
χ	amount of bonding	[-]
χ_0	initial amount of bonding	[-]
ψ	dilatancy angle	[°]
ω	absolute effectiveness of rotational hardening	[-]
ω_d	relative effectiveness of rotational hardening	[-]

Contents

List of Acronyms **ix**

Nomenclature **xi**

List of Figures **xvii**

List of Tables **xxi**

1 Introduction **1**
1.1 Background . . . 1
1.2 Aim and objectives . . . 2
1.3 Limitations . . . 3
1.4 Thesis structure . . . 3

2 Literature review **5**
2.1 Erosion of riverbanks . . . 5
2.2 Constitutive soil modelling . . . 7

3 Case study **17**
3.1 Ground conditions . . . 17
3.2 Results of previous investigations . . . 18

4 Numerical model **21**
4.1 Estimation of rate of erosion . . . 21
4.2 Model geometry . . . 21
4.3 Parameter determination . . . 23
4.4 Meshing . . . 25
4.5 Calculation stages . . . 25

5 Results and discussion **27**
5.1 Serviceability . . . 27
5.2 Stability . . . 31
5.3 Effect of erosion . . . 32
5.4 Impact on infrastructure . . . 34

6 Conclusions and recommendations **41**
6.1 Conclusions . . . 41
6.2 Recommendations . . . 42

A Additional case study information **I**
A.1 Sampling information I
A.2 Location of new buildings I

B Numerical model dimensions **III**

C Constitutive soil model parameters **VII**

D Numerical model meshes **IX**

E Post-processing locations **XI**

F Vertical displacements with time **XIII**

G Excess pore water pressure dissipation with time **XV**

H Horizontal displacement profiles **XVII**

I Change in displacements due to erosion **XXVII**

J Development of incremental deviatoric strains with time **XXIX**

K Effect on utilities **XXXI**

List of Figures

1.1 Location of the Nolhaga wastewater treatment plant. Image modified from Google (n.d.-b). 2

2.1 River cross section showing examples of erosion processes. 5
2.2 The Soft Soil Creep model. Image based on Karstunen and Amavasai (2017). 10
2.3 The Creep-SCLAY1S model in triaxial space. Image based on Gras et al. (2017a). 11

3.1 Overview of the Nolhaga site. Image modified from Google (n.d.-a). . 18
3.2 Locations of the chosen sections in the stability analysis. The red circle indicates the slope at risk of failure. Image modified from Google (n.d.-a). 19
3.3 Map over stretches with ongoing erosion, marked in orange. Image modified from Google (n.d.-a). 20

4.1 Map over the sections used in the analysis. The original sections can be seen in yellow, with the red lines indicating the extended parts of the sections used in this project. 22
4.2 Example of erosion pattern in section A. Each cut represents the eroded thickness at the different 50-year time steps. 23

5.1 Vertical displacement development over time for sections A and E using different constitutive models. 28
5.2 Excess pore water pressure dissipation over time for sections A and E using different constitutive models. 28
5.3 Section E horizontal displacements in the right cross section with the different constitutive models. 30
5.4 Development of safety factors over time for all sections. IC and AC on the time-axis stand for "initial conditions" and "after construction" respectively. These two phases are not in scale with the rest of the time steps. 31
5.5 Change in vertical displacements in sections C and E as a result of modelling erosion. 33
5.6 Change in horizontal displacements in sections C and E as a result of modelling erosion. 33

5.7 Section profile showing the locations of the developing incremental deviatoric strains after 400 years using the Creep-SCLAY1S model in section C. . . . 34
5.8 Incremental deviatoric strains with time below the middle of the building at approximately +37 m, using Creep-SCLAY1S, in sections A, C, and E. . . . 35
5.9 Map over the location of the analysed pipelines relative to the studied slope sections. Note that the pipelines are named left and right in relation to which side of the building they are in the section profiles, not on the map. . . . 36

A.1 Map over borehole locations (Google, n.d.-a). . . . II
A.2 Latest plan map over expected building placement at Nolhaga from Ramboll. . . . II

B.1 Sketch showing the dimensions the section A model, including applied loads. . . . III
B.2 Sketch showing the dimensions the section B model, including applied loads. . . . IV
B.3 Sketch showing the dimensions the section C model, including applied loads. . . . IV
B.4 Sketch showing the dimensions the section D model, including applied loads. . . . V
B.5 Sketch showing the dimensions the section E model, including applied loads. . . . V

D.1 Legend showing the colors of the different soil layers in the numerical models. . . . IX
D.2 Plaxis numerical model mesh for section A. . . . X
D.3 Plaxis numerical model mesh for section B. . . . X
D.4 Plaxis numerical model mesh for section C. . . . X
D.5 Plaxis numerical model mesh for section D. . . . X
D.6 Plaxis numerical model mesh for section E. . . . X

E.1 Post-processing locations for section A. . . . XI
E.2 Post-processing locations for section B. . . . XI
E.3 Post-processing locations for section C. . . . XII
E.4 Post-processing locations for section D. . . . XII
E.5 Post-processing locations for section E. . . . XII

F.1 Vertical displacement development over time for sections B, C, and D using different constitutive models. . . . XIII

G.1 Excess pore water pressure dissipation over time for sections B, C, and D using different constitutive models. . . . XV

H.1 Section A horizontal displacements in the left cross section with the different constitutive models. . . . XVIII

H.2 Section A horizontal displacements in the right cross section with the different constitutive models. . . . XIX
H.3 Section B horizontal displacements in the left cross section with the different constitutive models. . . . XX
H.4 Section B horizontal displacements in the right cross section with the different constitutive models. . . . XXI
H.5 Section C horizontal displacements in the left cross section with the different constitutive models. . . . XXII
H.6 Section C horizontal displacements in the right cross section with the different constitutive models. . . . XXIII
H.7 Section D horizontal displacements in the left cross section with the different constitutive models. . . . XXIV
H.8 Section D horizontal displacements in the right cross section with the different constitutive models. . . . XXV
H.9 Section E horizontal displacements in the left cross section with the different constitutive models. . . . XXVI

I.1 Change in vertical displacements in sections A, B, and D as a result of modelling erosion. . . . XXVII
I.2 Change in horizontal displacements in sections A, B, and D as a result of modelling erosion. . . . XXVIII

J.1 Section profile showing the locations of the developing incremental deviatoric strains after 400 years using the Creep-SCLAY1S model in section A. . . . XXX
J.2 Section profile showing the locations of the developing incremental deviatoric strains after 400 years using the Creep-SCLAY1S model in section E. . . . XXX

K.1 Location of the pipelines in section B. . . . XXXI
K.2 Location of the pipelines in section C. . . . XXXI
K.3 Location of the pipelines in section E. . . . XXXI
K.4 Horizontal and vertical displacement over time around the pipes to the left of the building in section B. . . . XXXII
K.5 Horizontal and vertical displacement over time around the pipes to the right of the building in section B. . . . XXXII
K.6 Horizontal and vertical displacement over time around the pipes to the left of the basin in section C. . . . XXXIII
K.7 Horizontal and vertical displacement over time around the pipes to the right of the basin in section C. . . . XXXIII
K.8 Horizontal and vertical displacement over time around the pipes to the left of the buildings in section E. . . . XXXIV
K.9 Horizontal and vertical displacement over time around the pipes to the right of the buildings in section E. . . . XXXIV

List of Tables

2.1 Input parameters for the considered constitutive soil models. 15

4.1 Expected total thickness of eroded material at each time interval. . . 22
4.2 Table showing all calculation phases in the Plaxis models. For the Creep-SCLAY1S models, the safety calculations are not run. 26

5.1 Ratio between calculated vertical and horizontal displacements, and assumed pipeline length when using the Mohr-Coulomb model. 37
5.2 Ratio between calculated vertical and horizontal displacements, and assumed pipeline length when using the Soft Soil Creep model. 37
5.3 Ratio between calculated vertical and horizontal displacements, and assumed pipeline length when using the Creep-SCLAY1S model. . . . 37
5.4 Ratio between calculated vertical and horizontal displacements in the non-erosion scenario, and assumed pipeline length when using the Mohr-Coulomb model. 38
5.5 Ratio between calculated vertical and horizontal displacements in the non-erosion scenario, and assumed pipeline length when using the Soft Soil Creep model. 38
5.6 Ratio between calculated vertical and horizontal displacements in the non-erosion scenario, and assumed pipeline length when using the Creep-SCLAY1S model. 38

C.1 General parameter values used for all constitutive soil models. VII
C.2 Parameter values used for the Mohr-Coulomb model. VII
C.3 Parameter values used for the Soft Soil Creep model. VIII
C.4 Parameter values used for the Creep-SCLAY1S model. VIII

1

Introduction

This chapter introduces the background of the studied problem, as well as the aim and limitation of the thesis. The overall structure of the report is also presented.

1.1 Background

As the effects of climate change has become more and more apparent, there is an increased necessity to predict potentially catastrophic events, and attempt to minimize their impacts. A part of this effort is being made in the field of geotechnics, where the changing temperatures and intensified precipitation affect the conditions in the ground (Kandalai et al., 2023). Changes in these conditions, if not properly accounted for, could lead to excessive ground movements, which in turn could result in economical costs in the form of damaged buildings and infrastructure. It could also trigger landslides, which in the worst case could cause loss of human life. However, a consequence that is often overlooked is the increased risk of erosion. Bank erosion along rivers is an example of this, where many different geomorphic processes in various ways remove material from the bank (Chassiot et al., 2020). The activities of some of these processes have become more frequent due to climate change, which in turn increases erosion rates. This can result in effects on the local ecological conditions, and thus affect the flora and fauna that surround the river. Since much of human activity tends to revolve around rivers, in the form of cities, shipping, hydro-power plants etc., the effects on infrastructure can be significant.

This thesis project is performed using data from a specific case study. The site is located in the area of Nolhaga in the city of Alingsås, where there are plans to construct a new wastewater treatment plant. See Figure 1.1 for a map of the area. The current plans for the new Nolhaga treatment plant include the construction of buildings close to the banks of the river south of the site. Preliminary stability analyses have been performed on five different slope sections in the area. They indicate that all but one of the sections are safe from failure. The investigations also establish the presence of slope erosion, and point out the many potential issues associated with such processes. However, due the difficulties in predicting and modelling erosion, no conclusions have been made on how potential future erosion will affect the slope stability in the area.

Figure 1.1: Location of the Nolhaga wastewater treatment plant. Image modified from Google (n.d.-b).

There are several studies dealing with the origins and effects of riverbank erosion. None, however, consider the influence of soil properties such as creep, anisotropy and structural degradation can have on this process, and how this in turn affects buildings close to the banks. Therefore, this thesis aims to use advanced constitutive soil models in order to estimate these effects. A finite element (FE) approach using *PLAXIS 2D* is chosen for this task. Three different constitutive models with varying complexity are used and compared in order to determine the variations in the received results, depending on the modelled behaviour of the soil. The three constitutive soil models that are chosen for this analysis are Mohr-Coulomb, Soft Soil Creep, and Creep-SCLAY1S. These models are chosen because of their relevance in real-life applications. Mohr-Coulomb is the model that is most used in the industry, whereas Soft Soil Creep and Creep-SCLAY1S have the potential to capture the behaviour of soft soil more accurately.

1.2 Aim and objectives

The aim of the thesis is to investigate with the help of numerical analyses how the potential river erosion might affect the buildings and pipelines in Nolhaga wastewater treatment plant in Alingsås.

The objective of this thesis is as follows:

- Analyze the variations in predicted displacements and safety factors when using different constitutive models, and how they evolve with time.
- Investigate the influence of erosion on the stability and serviceability of the infrastructure (both long and short term) using different constitutive soil models.

1.3 Limitations

- No new field measurements or lab tests are performed within the scope of this project. Therefore, soil parameters are determined based on the tests already performed at the site, with empirical data being used where site-specific information is missing.
- There is no site-specific information regarding the erosion patterns at the site, or their causes. Instead, these have to be assumed based on available literature.
- The analysis is limited to the five slope sections already established at the site. No new sections are studied within the scope of this work.

1.4 Thesis structure

The thesis begins with a literature review, presented in Chapter 2. This review gives information on the mechanisms of bank erosion, as well as what has been done in previous studies. The chapter also establishes the background and formulations of the constitutive soil models used in the project, and the advantages and disadvantages with each of them. The thesis continues with Chapter 3, which gives more information about the study area, and goes through relevant results of the previous investigations performed at the site. Chapter 4 then describes the set-up of the numerical model, and derived parameters for each of the constitutive soil models. The results of the analyses are presented and discussed in Chapter 5, and the conclusions and recommendations based on these results are then reported in Chapter 6.

2

Literature review

This chapter includes a brief summary of some basic concepts related to riverbank erosion, as well as a discussion on what aspects of bank erosion that has been analysed in previous studies. It also contains information on the theoretical formulations of the different constitutive soil models used in this thesis, and their respective positive and negative aspects.

2.1 Erosion of riverbanks

Bank erosion can have large effects on surrounding ecological and anthropogenic activity (Islam & Guchhait, 2024). It can destroy houses and infrastructure, causing severe socioeconomic consequences. Since many important societal functions are located along the banks of rivers, such as water treatment plants, fishing industries, and agriculture, it is of great interest to predict and prevent the effects of erosion in order to protect these assets (Chassiot et al., 2020).

Riverbank erosion can be affected by many different factors, depending on the local site conditions, see Figure 2.1. One of the main factors is the effects of the water flowing in the river (Jugie et al., 2018; Luppi et al., 2009; Hooke, 1979). Both the flow and the occurrence of waves on the water can break away soil particles from the riverbank, thus causing erosion. In northern environments such as Sweden, the

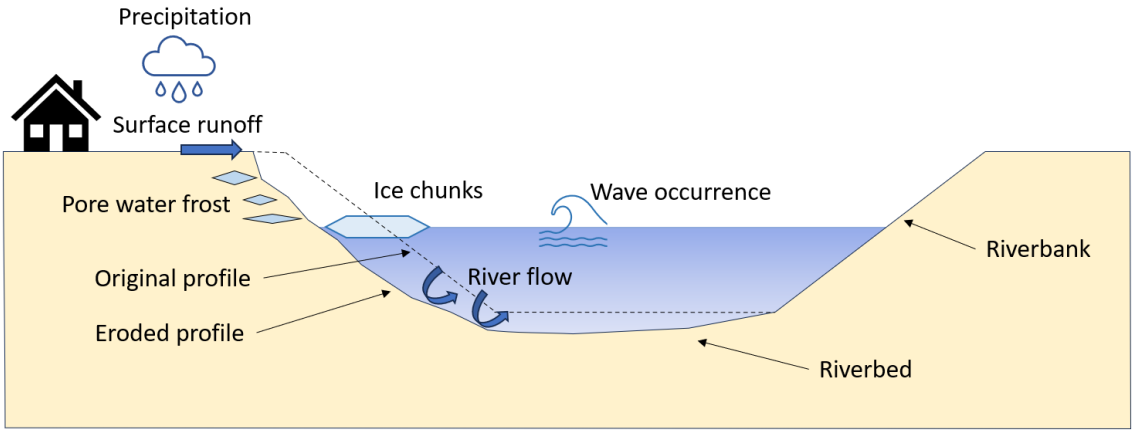

Figure 2.1: River cross section showing examples of erosion processes.

formation of ice also plays a key role in bank erosion (Chassiot et al., 2020). Ice chunks transported by the river can both scrape up against the shores of the riverbanks, and cause ice-dams which can create floods. Additionally, ice forming in the pore water of the soil due to frost can cause disturbances in the soil structure, making it more vulnerable to other erosive processes (Chassiot et al., 2020). Precipitation is another factor that can affect erosion both directly and indirectly (Jugie et al., 2018). Simply the impact of the raindrops can have a weathering effect on the bank, as well as the surface runoff that rainfall events create. In the long-term, rainwater can break up bonds and, like frost, weaken the riverbank which promotes further erosion. Riverbank erosion is incredibly difficult to predict, since the factors that affect it are extremely dynamic (Hooke, 1979). Therefore, in order to have a reasonable idea of the erosion behaviour at a particular site, the information on these factors, and their variability, have to be known.

Previous studies related to bank erosion focus on several different aspects of the process. However, due to the inherent variability of the parameters that affect riverbank erosion, many of the studies attempt to determine relevant influential factors at certain sites, and establish relationships between their values and the expected erosion behaviour. There are several different approaches that have been used to achieve this. One such approach is using statistical regression analysis on collected data of parameters such as river flow velocity and precipitation amounts, and comparing those with measured slope erosion in order to find correlations between them. One of the more famous papers related to this is by Hooke (1979), but several, other examples exist, such as ones by Lawler (1986), Jugie et al. (2018), and Saadon et al. (2021).

Another methodology is through the use of numerical analyses, and in that way investigate the effects that different parameter values have on the expected behaviour of bank erosion. Darby et al. (2007) used the programs *SEEP/W* and *SLOPE/W* to perform an analysis of bank erosion, where the effects of fluvial erosion, pore water pressure changes, and slope stability were fully coupled. The fluvial erosion was modelled by manually changing the model mesh at the end of each time step, based on comparing the current shear stress caused by the river flow, and the shear strength of the riverbank soil. Pore pressure changes were then modelled by finite element seepage in *SEEP/W*, and the slope stability analysis was subsequently performed in *SLOPE/W*. If the safety factor fell below 1, the mesh was again manually changed, this time to simulate a mass failure, before continuing with the next time step. In this way, the erosion patterns of the slope could be modelled. El Kadi Abderrezzak et al. (2016) also incorporated numerical analysis to simulate bank erosion, using the program *TELEMAC-2D* to calculate water velocity and depth, and the program *SISYPHE* to calculate bank evolution as a result of slope failure. However, they made use of an algorithm that compared the inclination of each element in the mesh to a specified angle of repose of the soil material instead . If the slope angle was steeper than the angle of repose, it simulated bank failure by changing the mesh and lowering the inclination, while still preserving mass balance in the system.

However, none of these studies analyse the effect that erosion can have on sur-

rounding structures. They also do not consider the effects of soil properties such as anisotropy, structural degradation, and creep. This is seen as a relevant topic to investigate, since accounting for these properties allows for an analysis that is more true to actual soil behaviour, and could have a large impact on the accuracy of erosion modelling. This thesis therefore makes use of advanced constitutive soil models in the FE-software *PLAXIS 2D* to account for these properties.

Another aspect that is not investigated in any previous study is the differences in the expected erosion effects depending on what constitutive soil model is used. Since simpler models disregard many integral aspects of soil behaviour, the results can either be more or less conservative compared to using complex models. It is therefore important to explore these differences in order to have a better understanding of the strengths and shortcomings of the models in the context of the analysed scenario. Because of these aspects, a comparison is made in this thesis between three different constitutive soil models, ranging from simple to complex in formulation. The following chapter presents the chosen models.

2.2 Constitutive soil modelling

In this chapter, the theoretical background to the constitutive models used in this thesis are presented.

2.2.1 Mohr-Coulomb

The Mohr-Coulomb (MC) constitutive model is an elastic-perfectly plastic model (Muir Wood, 2004). The yield function for this model can be defined in terms of principal stresses σ'_1 and σ'_3 as follows in Equation 2.1:

$$f(\vec{\sigma'}) = (\sigma'_1 - \sigma'_3) - (\sigma'_1 + \sigma'_3)sin\varphi' - 2c'cos\varphi' = 0 \tag{2.1}$$

where the strength parameters c' and φ' are the effective cohesion and friction angle respectively, and $\vec{\sigma'}$ is a six component vector of Cartesian stresses. The function can be reworked to be defined in terms of mean effective stress, p', and deviatoric stress, q instead, as seen in Equation 2.2:

$$f(\vec{\sigma'}) = f(p', q) = q - Np' - c^* = 0 \tag{2.2}$$

where N and c^* are soil properties, defined in Equation 2.3 below (Muir Wood, 2004).

$$N = \frac{6sin\varphi'}{3 - sin\varphi'} \qquad\qquad c^* = \frac{6c'cos\varphi'}{3 - sin\varphi'} \tag{2.3}$$

Furthermore, p' and q can be related to the volumetric and deviatoric elastic strains, $d\varepsilon_v^e$ and $d\varepsilon_q^e$ respectively, by Equation 2.4:

$$\begin{Bmatrix} dp' \\ dq \end{Bmatrix} = \begin{bmatrix} K' & 0 \\ 0 & 3G' \end{bmatrix} \begin{Bmatrix} d\varepsilon_v^e \\ d\varepsilon_q^e \end{Bmatrix} \tag{2.4}$$

where K' is the effective bulk modulus, defined as $K' = \frac{E'}{3(1-2\nu')}$, and G' is the effective shear modulus, defined as $G' = \frac{E'}{2(1+\nu')}$. In both these definitions, E' is the effective Young's modulus and ν' is Poisson's ratio.

The plastic potential function, g, is defined in Equation 2.5 as follows (Muir Wood, 2004):

$$g(\vec{\sigma'}) = g(p', q) = q - N^* p' + k = 0 \tag{2.5}$$

where k is a variable with an arbitrary value that allows the function to be defined at the current stress state, and N^* is a soil property defined by the dilatancy angle ψ, and is formulated in Equation 2.6:

$$N^* = \frac{6sin\psi}{3 - sin\psi} \tag{2.6}$$

The consistency condition in the MC model is defined by Equation 2.7:

$$df = \frac{\partial f}{\partial p'} dp' + \frac{\partial f}{\partial q} dq = 0 \tag{2.7}$$

By using the equations defined above, the relationship between the changes in stress and the changes in strain for the MC model can be defined as Equation 2.8:

$$\begin{Bmatrix} dp' \\ dq \end{Bmatrix} = \left(\begin{bmatrix} K' & 0 \\ 0 & 3G' \end{bmatrix} - \frac{1}{K'NN^* + 3G'} \begin{bmatrix} NN^*K'^2 & -3N^*G'K' \\ -3NG'K' & 9G'^2 \end{bmatrix} \right) \begin{Bmatrix} d\varepsilon_v \\ d\varepsilon_q \end{Bmatrix} \tag{2.8}$$

2.2.2 Soft Soil Creep

The Soft Soil Creep (SSC) model (Vermeer et al., 1998; Vermeer and Neher, 1999) was developed from the Soft Soil (SS) model. The SS model was, in turn, based on the Modified Cam Clay (MCC) model (Roscoe & Burland, 1968).

The SSC model is a rate-dependant model, and as such has a different model formulation compared to the SS model. This is because the model accounts for

creep. Creep becomes a component in the developing irrecoverable strains, since all creep strains are considered irrecoverable. Creep is constantly occurring, regardless of where the stress state is currently located, which means that visco-plastic strains are always developing. This, in turn, entails that there is no purely elastic region in the model, and the yield surface instead becomes the boundary between small and large irrecoverable creep strains (Karstunen & Amavasai, 2017). Therefore, instead of calling the bounding surface a yield surface, it is referred to as the Normal Compression Surface (NCS), and the magnitude of the creep strains is dependant on the proximity of the current stress state to the NCS.

The volumetric strain increment, $d\varepsilon_v$ is similarly to the elasto-plastic models split into an elastic and a viscoplastic (creep) strain part, $d\varepsilon_v^e$ and $d\varepsilon_v^c$ respectively. The elastic part is defined according to the elastic law of the SSC model, and can be seen in Equation 2.9. The flow is assumed to be associated. The volumetric creep strain are calculated using Equation 2.10:

$$d\varepsilon_v^e = \kappa^* \frac{dp'}{p'} \tag{2.9}$$

$$d\varepsilon_v^c = \frac{\mu^*}{\tau} \left(\frac{p'_{eq}}{p'_p} \right)^{\beta}, \qquad \beta = \frac{\lambda^* - \kappa^*}{\mu^*} \tag{2.10}$$

where λ^* is the modified compression index, κ^* is the modified swelling index, and μ^* is the modified creep index. The parameter τ is a reference time, implicitly assumed to be one day, and is related to the loading rate that is used when defining the apparent preconsolidation pressure. The ratio $\frac{p'_{eq}}{p'_p}$ is a triaxial equivalent of the inverse of the overconsolidation ratio (OCR), and controls the creep strain rate at the current stress state. The current stress state is related to p'_{eq}, and p'_p is called the isotropic preconsolidation pressure and is used to define the NCS, see Figure 2.2. This means that as the stress state gets closer to the NCS, the value of p'_{eq} will get closer to p'_p, and thus the ratio gets closer to 1 and the creep strain rate increases. The relation between the current stress state and p'_{eq} is defined in Equation 2.11 as:

$$p'_{eq} = p' + \frac{q^2}{M^* \, p'} \tag{2.11}$$

where M^* is a parameter that is determined by the input value of the coefficient of lateral earth pressure at rest under normally consolidated conditions, K_0^{NC}. Like the yield surfaces in the MCC and SS models, the NCS is defined as an ellipse, with the aspect ratio being controlled by M^*, and the size being controlled by p'_p. The current stress state can also be seen as always lying on an elliptic surface, here called the current stress surface (CSS), see Figure 2.2, whose aspect ratio is also defined by M^*. However, the size of the CSS is instead defined by p'_{eq}, which means that the closer that p'_{eq} gets to p'_p, the closer the CSS gets to the NCS.

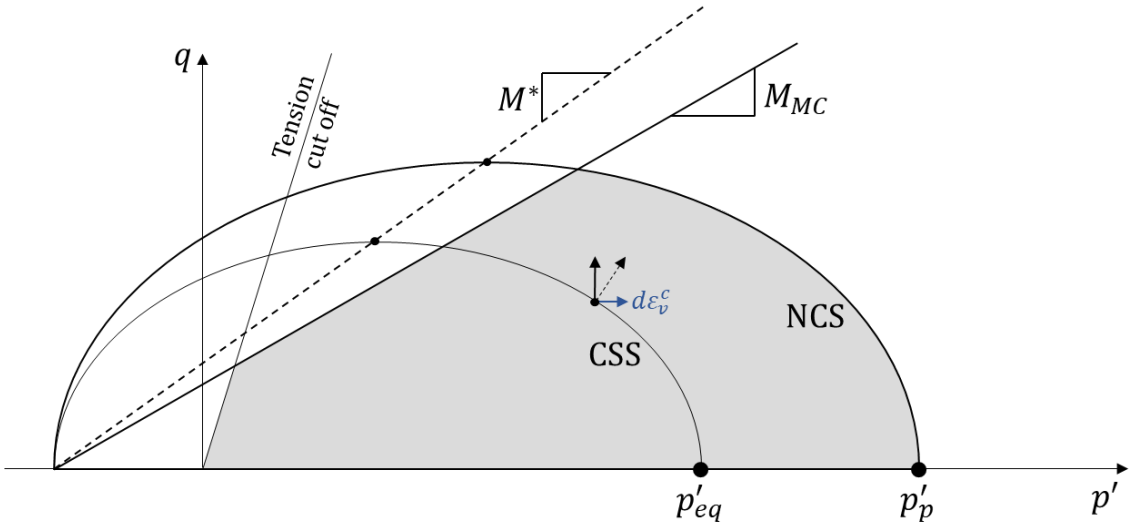

Figure 2.2: The Soft Soil Creep model. Image based on Karstunen and Amavasai (2017).

The parameter p'_p is defined by the model's hardening law, which can be seen in Equation 2.12 below:

$$p'_p = p' exp\left(\frac{d\varepsilon_v^p}{\lambda^* - \kappa^*}\right) \tag{2.12}$$

The failure condition in the SSC model is defined by the Mohr-Coulomb failure criterion, formulated in equation 2.1. No strain softening is allowed in the SS and SSC models. This is because strain softening creates severe issues during finite element analysis, such as mesh dependency and convergence problems (Karstunen & Amavasai, 2017). Stress states are therefore not allowed above the Mohr-Coulomb failure line, noted as M_{MC} in Figure 2.2, in these models.

2.2.3 Creep-SCLAY1S

The Creep-SCLAY1S model is an anisotropic creep model, featuring bonding and destructuration. It is an extension of the Creep-SCLAY1 model proposed by Sivasithamparam et al. (2015), that in turn builds on concepts and models developed by Wheeler et al. (2003), Karstunen et al. (2005), and Leoni et al. (2008). Further investigations into parameter calibration and ranges have also been performed by Gras et al. (2017a) and Gras et al. (2017b).

The definition of the Creep-SCLAY1S model is originally formulated using a deviatoric stress vector, $\vec{\sigma}_d$, instead of the deviator stress, q, in order for the model to be defined in general stress space. However, for the sake of simplicity, it is in this thesis defined in triaxial stress space, which simulate triaxial tests on a soil sample cut vertically from the soil (Sivasithamparam et al., 2015). See Figure 2.3 for an overview of the model in triaxial stress space. The equation for the NCS can then

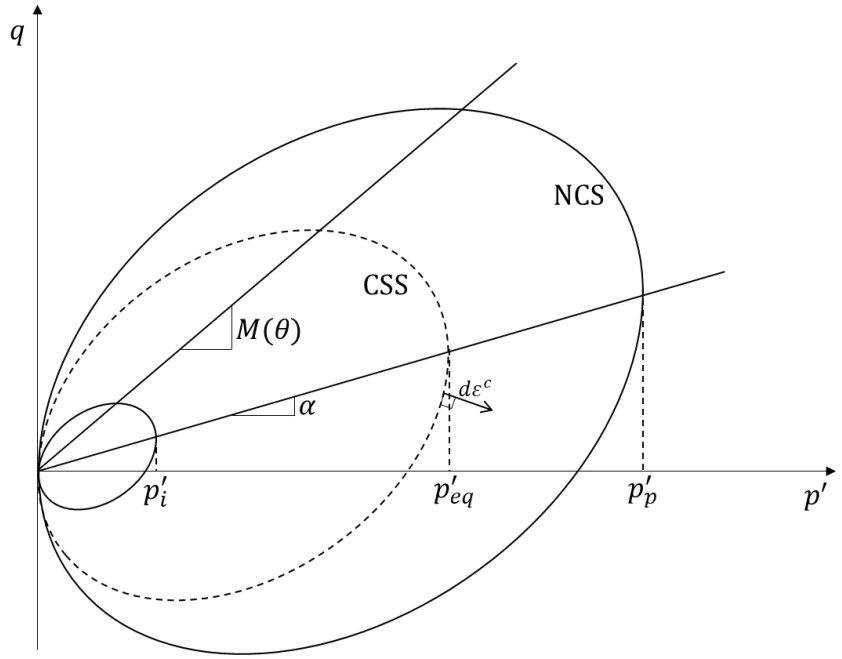

Figure 2.3: The Creep-SCLAY1S model in triaxial space. Image based on Gras et al. (2017a).

be written as follows in Equation 2.13:

$$f_{NCS} = (q - \alpha p')^2 - \left(M(\theta)^2 - \alpha^2\right)\left[p'_p - p'\right]p' = 0 \tag{2.13}$$

where α is a scalar in this triaxial definition, but a state variable in the general formulation, and is used to describe the inclination of the NCS. M is the stress ratio at critical state, here dependent on the Lode angle, θ, which makes it possible to have different stress ratios in triaxial compression, M_c, and extension, M_e. The parameter p'_p is, just as in the SSC model, used to define the size of the NCS, and is initially defined using the OCR or pre-overburden pressure (POP) value. The shape and inclination of the CSS is identical to the NCS. The size, however, is defined by p'_{eq}, the formulation of which is similar to the one in SSC, see Equation 2.11, just with the addition of accounting for anisotropy. See Equation 2.14:

$$p'_{eq} = p' + \frac{(q - \alpha p')^2}{(M^2(\theta) - \alpha^2)\, p'} \tag{2.14}$$

The model features a third surface, seen as the smallest surface in Figure 2.3. This surface is called the Intrinsic Compression Surface (ICS) and is an imaginary surface that represents the NCS of the soil without any bonds, but with the same void ratio. It is used in the model to account for the effects of bonding in the soil. The surface has the same shape and inclination as the NCS but has a smaller size determined by a parameter p'_i. This parameter is defined by a relationship related

to the sensitivity of the soil, S_t, represented by the current amount of bonding, $\chi = S_t - 1$. The relation is formulated in Equation 2.15 below:

$$p'_p = (1 + \chi)p'_i \tag{2.15}$$

When it comes to flow rules, the Creep-SCLAY1S model assumes an associated flow. This is seen as a reasonable assumption for natural clays, as the model takes anisotropy into account (Wheeler et al., 2003). The change in volumetric and deviatoric creep strains are therefore formulated in Equation 2.16 as follows:

$$d\varepsilon_v^c = d\Lambda \frac{\partial p'_{eq}}{\partial p'} \qquad\qquad d\varepsilon_q^c = d\Lambda \frac{\partial p'_{eq}}{\partial q} \tag{2.16}$$

where $d\Lambda$ is the viscoplastic multiplier, defined in Equation 2.17 as:

$$d\Lambda = \frac{\mu_i^*}{\tau} \left(\frac{p'_{eq}}{p'_p} \right)^{\beta} \left(\frac{M_c^2 - \alpha_{K0}^2}{M_c^2 - \eta_{K0}^2} \right), \qquad\qquad \beta = \frac{\lambda_i^* - \kappa^*}{\mu_i^*} \tag{2.17}$$

where μ_i^* is the modified intrinsic creep index, and λ_i^* is the modified intrinsic compression index. The value of these parameters can be derived the same way as the non-intrinsic variants, but instead on a sample where all bonding in the soil has been destroyed (Karstunen & Amavasai, 2017). The τ parameter is the reference time, and like in the SSC model referring to the duration of the load increment in the test used to derive the preconsolidation pressure. The η parameter is the stress ratio $\eta = q/p'$, and the subscript $K0$ refers to the value of those parameters in normally consolidated K_0 state.

The Creep-SCLAY1S model has three hardening laws that account for different hardening processes: one that controls the size of the ICS (and subsequently also the NCS), one that controls the degradation of bonding, and one that controls the evolution of anisotropy. The change in size of the ICS is determined by the change in volumetric creep rate, and is defined by Equation 2.18:

$$dp'_i = \frac{p'_i d\varepsilon_v^c}{\lambda_i^* - \kappa^*} \tag{2.18}$$

The degradation of bonding is determined by the change in both volumetric and deviatoric creep strains, and is defined in Equation 2.19 as follows:

$$d\chi = -\zeta\chi \left[|d\varepsilon_v^c| + \zeta_d \left(d\varepsilon_q^c \right) \right] \tag{2.19}$$

where ζ is the absolute rate of destructuration and ζ_d is the relative rate of destructuration. $|d\varepsilon_v^c|$ is the absolute value of the volumetric creep strain. The evolution of anisotropy results in the rotation of the three defined surfaces, and is also related to the changes in volumetric and deviatoric creep strains. The relation is formulated in Equation 2.20 below:

$$d\alpha = \omega \left[\left(\frac{3\eta}{4} - \alpha \right) \langle d\varepsilon_v^c \rangle + \omega_d \left(\frac{\eta}{3} - \alpha \right) |d\varepsilon_q^c| \right] \tag{2.20}$$

where the Macaulay brackets, $\langle\rangle$, mean that $\langle d\varepsilon_v^c \rangle = 0$ if $d\varepsilon_v^c < 0$ and $\langle d\varepsilon_v^c \rangle = d\varepsilon_v^c$ if $d\varepsilon_v^c \geq 0$. ω is the absolute effectiveness of rotational hardening, and ω_d is the relative effectiveness of rotational hardening.

2.2.4 Summary

The MC model is commonly used in the industry due to its (perceived) simplicity (Muir Wood, 2004). However, because of this simplicity, the model has many drawbacks that makes it less suitable to use compared to more advanced constitutive models. For example, the model's yield surface in principal stress space is an irregular hexagon with sharp edges that causes numerical issues during computation. The model also predicts linear elastic deformations, something which is not true to real soil behaviour, and gives unrealistically high predictions of heave during excavation (Muir Wood, 2004). Additionally, the model assumes that the soil behaves perfectly plastic, without any hardening or softening, which is also not realistic. Finally, according to the model when the soil is yielding, the volumetric strain are either negative (constant dilation) or zero (zero dilation).

The SSC model has many advantages over the MC model in representing the response of soft soils. For example, the model includes a hardening law, which accounts for the effects of stress history on soil stiffness. The SSC model also predicts non-linear elasticity, which is more in line with real soil behaviour (Karstunen & Amavasai, 2017). Another significant advantage of the SSC model is the inclusion of creep, which can have a large impact on the expected displacements of the model. However, the SSC model contains flaws of its own. For example, since no strain softening is allowed, the model is not appropriate to represent heavily overconsolidated clays, which tend to show a softening response when sheared (Karstunen & Amavasai, 2017). This further means that the model is not suitable for unloading problems. The SSC model also overestimates the magnitude of creep strains by assuming that the NCS is the contour of constant volumetric creep strains (Karstunen & Amavasai, 2017). Additionally, the model does not account for anisotropy and structural degradation, something that is very prevalent in natural soft clays.

In contrast, the effects of anisotropy is accounted for in the Creep-SCLAY1S model (Karstunen & Amavasai, 2017). The model also accounts for the evolution of anisotropy that occurs during changes in loading directions. Additionally, the model includes the effects of bonding in natural soils, and the subsequent degradation of

these bonds (destructuration) due to (irrecoverable) creep straining (Karstunen & Amavasai, 2017). Furthermore, the Creep-SCLAY1S model assumes a constant total creep rate, instead of the constant volumetric creep rate present in the SSC model. In both SSC and Creep-SCLAY1S, no consistency condition is defined, which means that stress states are allowed outside of the NCS. The soil can then be regarded as "under-consolidated", and large creep strains develop as a result. The biggest issue with the Creep-SCLAY1S model is that it requires the knowledge of significantly more parameters, compared to the other two models (Karstunen & Amavasai, 2017). This makes it less user-friendly, since it means that more parameters have to be defined. The parameters required for each constitutive model is summarized in Table 2.1.

Table 2.1: Input parameters for the considered constitutive soil models.

Constitutive model	Parameter	Description	Unit
Mohr-Coulomb	E'_{ref}	Reference effective Young's modulus	kN/m^2
	ν'	Poisson's ratio	-
	c'_{ref}	Reference effective cohesion	kN/m^2
	φ'	Friction angle	$^\circ$
	ψ	Dilatancy angle	$^\circ$
Soft Soil Creep	λ^*	Modified compression index	-
	κ^*	Modified swelling index	-
	μ^*	Modified creep index	-
	ν'_{ur}	Poisson's ratio for unloading-reloading	-
	c'_{ref}	Reference effective cohesion	kN/m^2
	φ'_{cv}	Critical state friction angle	$^\circ$
	ψ	Dilatancy angle	$^\circ$
	K_0^{NC}	Coefficient of lateral earth pressure at rest under normally consolidated conditions	-
	OCR/POP	Overconsolidation ratio *in situ*/Pre-overburden pressure	- / kN/m^2
Creep-SCLAY1S	κ^*	Modified swelling index	-
	ν'_{ur}	Poisson's ratio for unloading-reloading	-
	λ_i^*	Modified intrinsic compression index	-
	M_c	Critical state stress ratio in compression	-
	M_e	Critical state stress ratio in extension	-
	ω	Absolute effectiveness of rotational hardening	-
	ω_d	Relative effectiveness of rotational hardening	-
	ζ	Absolute effectiveness of destructuration	-
	ζ_d	Relative effectiveness of destructuration	-
	OCR/POP	Overconsolidation ratio *in situ*/Pre-overburden pressure	- / kN/m^2
	e_0	Initial void ratio	-
	α_0	Initial inclination of yield surface	-
	χ_0	Initial amount of bonding	-
	τ	Reference time	days
	μ_i^*	Modified intrinsic creep index	-

3

Case study

The case study area is the construction site of a new wastewater treatment plant, located in the area of Nolhaga in the city of Alingsås. The purpose of the new plant is to replace the old one currently in use. To the south of the site runs a river called Säveån, and to the west lies the lake of Mjörn, which the river flows into. North of the site there is a nature reserve and a park called Kongo, and to the east there is an allotment area. See Figure 3.1 for a map of the site.

The details on the sampling previously performed at the site is available in Appendix A.1, and one of the latest plan maps over the expected building placement is presented in Appendix A.2. This plan map was not available when the initial geotechnical analyses were performed by Ramboll. However, it is used in this project when estimating the location and distribution of the applied loads in the slope sections, to get a more accurate view of the future conditions in the area. The following investigation reports of the Nolhaga treatment plant area have been used to gather information on the site:

- Nolhaga reningsverk, Markteknisk undersökningsrapport/ MUR Geo, Performed by Ramboll, from 2021-02-15
- Nolhaga reningsverk, PM Geoteknik, Performed by Ramboll, from 2021-03-05
- Nolhaga reningsverk, PM Stabilitet, Performed by Ramboll, from 2023-02-07

3.1 Ground conditions

The ground level of the site varies between +60 and +61 (RH2000), with the lowest point in the river being around level +52. The slopes from the site down to the river vary between 1:1.4 and 1:4.5 in inclination. In general, the soil profile is described as a 10-20 m deep layer of post-glacial sand underlain by a 26-33 m deep layer of glacial clay. The sand contains local layers of finer silty materials of varying thicknesses, which is assumed to be due to the historical meandering of the river. Below the clay there is a layer of frictional material, which in turn rests on bedrock. The thickness of this frictional layer and the depth of the bedrock surface are yet to be investigated. The pore water pressure measurements indicate a groundwater level of between 1.6-2.8 m below ground surface.

Figure 3.1: Overview of the Nolhaga site. Image modified from Google (n.d.-a).

3.2 Results of previous investigations

The following chapters present information on results from the previous investigations conducted at the site that is relevant to this thesis.

3.2.1 Stability analysis

Stability analyses of five selected riverbank slope sections were performed by Ramboll. The location of the analysed sections can be seen in Figure 3.2. The analyses were made in the program *SLOPE/W*. The results showed that sections A, B, C and E have satisfactory safety factors against failure. Section D was only deemed to have a sufficiently high safety factor within the boundaries of the local plan. However, the riverbank slope that is outside of these boundaries was assessed to be at risk of failure, see the red circled area in Figure 3.2. The safety factor of the riverbank slope was calculated to be 0.85, where a value of 0.8 and below is stated to imply a direct risk of failure. It was mentioned that since the slope is outside the boundaries of the local plan, it would not be addressed in the current construction project. Instead, it was recommended to the municipality that it should be remediated in some way, since it seems to be at high risk of failure.

3.2.2 Erosion assessment

Ramboll conducted a field investigation to catalogue any occurrence of erosion along the riverbanks closest to the site. It was concluded that there are stretches with ongoing erosion within the studied area. See Figure 3.3 for a map over the locations of these stretches. It was also discussed that because of the fact that Säveån is a meandering river, and the presence of fine-grained material in the soil, there is a

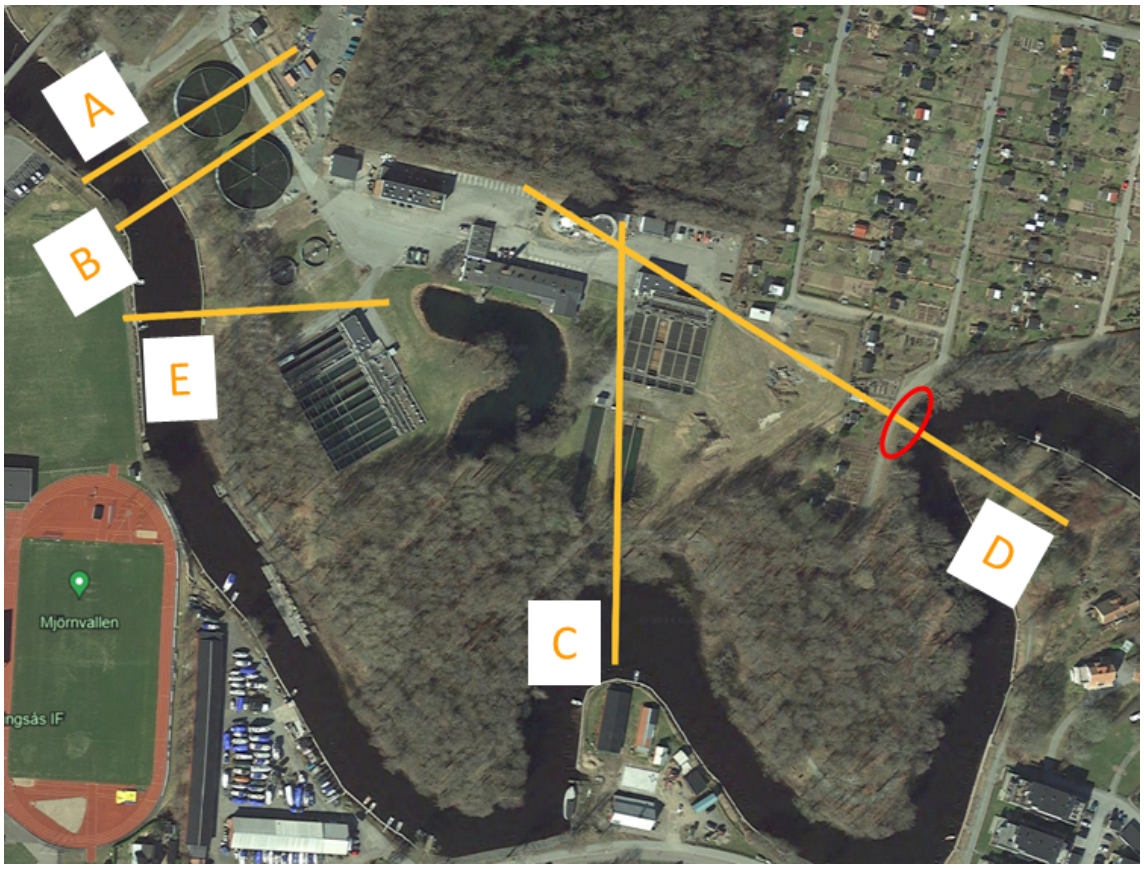

Figure 3.2: Locations of the chosen sections in the stability analysis. The red circle indicates the slope at risk of failure. Image modified from Google (n.d.-a).

high risk for erosion to start occurring along new stretches of the bank. Additionally, it was stated that the erosion could get intensified by climate change and a more frequent occurrence of extreme weather. Furthermore, it was speculated that since erosion protection has been installed on the southern side of the river, it could alter the river flow patterns, which in turn also could lead to erosion along new areas of the riverbank. However, due to the difficulties associated with predicting and modelling erosion, and how it may affect the geometry and subsequent stability of the slopes, it was not possible to give clear recommendations on how to deal with this issue.

Figure 3.3: Map over stretches with ongoing erosion, marked in orange. Image modified from Google (n.d.-a).

4

Numerical model

This chapter presents and explains the different aspects of the created numerical models.

4.1 Estimation of rate of erosion

Due to the lack of relevant site data, the rate of erosion is estimated based on an investigation of Säveån performed by the Swedish Geotechnical Institute (SGI) (SGI, 2017). Even though the part of the river that runs past Nolhaga was not included in this report, it is used as a best approximation for this project. A mean value is taken from the erosion intervals that were estimated in the report, which corresponds to an erosion rate of approximately 1.2 cm/year. For the sake of simplicity, this rate is assumed for all the analysed slope sections, even though in reality the meandering of the river likely leads do differences in the local flow patterns, and in turn varying erosion rates.

4.2 Model geometry

The geometries for the sections are based on the *SLOPE/W* files used during the initial stability assessment performed by Ramboll. However, they are altered in various ways. The ground surface and soil layering in each section are simplified to be completely flat, so that the "*K0 procedure*" in Plaxis can be used to generate initial stresses (Bentley, 2023). The analysed sections are also extended horizontally in order to avoid boundary effects in the simulations. See Figure 4.1 for the site plan map featuring the extended sections. Any additional buildings introduced into the section as a result of these extensions are added to the model to increase result accuracy. Section E is extended to include the pond present at the site, see Figure 4.1, which is modeled based on data from the area.

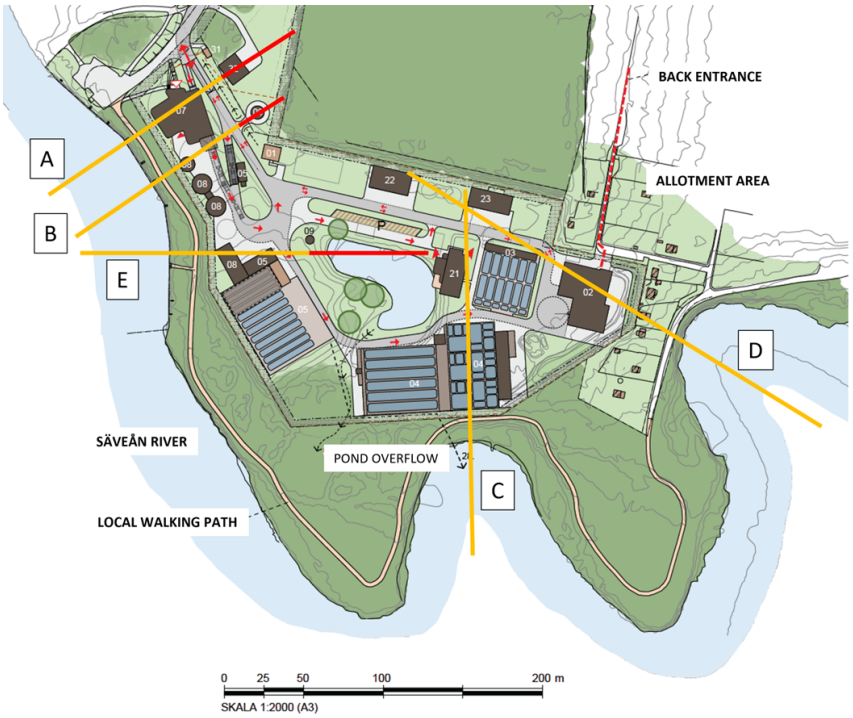

Figure 4.1: Map over the sections used in the analysis. The original sections can be seen in yellow, with the red lines indicating the extended parts of the sections used in this project.

To simulate the process of erosion acting on the slopes, the geometries are cut with a certain thickness, depending on how much time is said to have passed. The analysed time intervals are: 50, 100, 150, 200, 250, 300, 350, and 400 years. The expected total thickness of eroded material at each of the time intervals based on the assumed rate of erosion is presented in Table 4.1.

Table 4.1: Expected total thickness of eroded material at each time interval.

Passed time [years]	Total thickness [m]
50	0.6
100	1.2
150	1.8
200	2.4
250	3
300	3.6
350	4.2
400	4.8

A simplified erosion pattern is assumed, where the defined thicknesses are removed equally across the entire riverbed that is below the water surface. The soil in the banks on each side of the river are assumed to erode starting from where they intersect with the water surface and then expand outward, away from the water, at

the rate specified in Table 4.1. See Figure 4.2 for an example of how the erosion has been modelled in Section A.

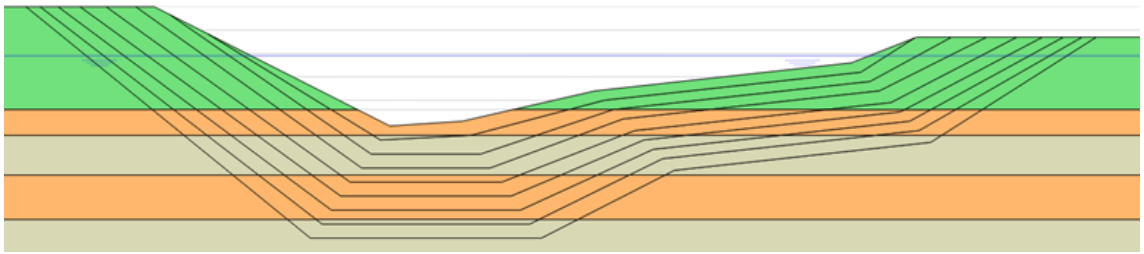

Figure 4.2: Example of erosion pattern in section A. Each cut represents the eroded thickness at the different 50-year time steps.

4.2.1 Water table

The water tables are based on the measurements from the site. The river water level is assumed to be the same as in the *SLOPE/W* calculations, and therefore set to +57.4 (RH2000). The pond water level in section E is set to +59 based on site measurements. The boundary conditions for the groundwater flow are assumed open on the sides and top of the section models, and closed on the bottom.

4.2.2 Applied loads

The building loads applied in each section are based on the ones used in the *SLOPE/W* calculations, except in sections C and D, where more recent load estimations for the project have been received. Where information is missing, the loads are set based on the assumed function of the corresponding structure. Since specific ground improvements below the planned buildings have not been decided on at the time of writing this thesis, no such features are included in the models.

The dimensions of the final geometries used in the analysis, including load distributions, are presented in Appendix B.

4.3 Parameter determination

In the following chapters, the methods used to derive the different constitutive model parameters are presented. Any parameter not mentioned is kept as the default value assigned in Plaxis. The drainage type for sand and silt is set to drained, and for clay set to undrained for all constitutive models. All of the assigned values are summarised in Appendix C.

4.3.1 General parameters

The unit weights, γ, for all the soils are based on the ones assumed by Ramboll in the initial stability analyses. The permeabilities, k, of the sand and silt are based

on standard values from SGI and assumed to be isotropic (Larsson, 2008). The permeability of the clay is derived from the CRS-tests performed at the site.

4.3.2 Mohr-Coulomb

The friction angles of the soils, φ', are derived from the values used in the Ramboll stability analyses. The effective cohesion, c', for the clay is also based on these analyses, which means it increases with depth starting from 20 m below ground level. For the silt, the effective cohesion is assumed to be 1 kPa. The cohesion for the sand is set to 1.5 kPa to keep some of the sections from failing under natural conditions. Young's modulus, E'_{ref}, is based on empirical data (Geotechdata.info, 2013). Poisson's ratio, ν', is assumed to be 0.2 for all soils. The in situ K_0 for clay is manually set to 0.6.

4.3.3 Soft Soil Creep

The friction angle and cohesion are set to the same values as in the MC model. The values for the modified compression index, λ^*, and the modified swelling index, κ^*, are derived based the CRS-tests from the site. However, due to the resulting values being deemed unreasonable, likely as a result of poor test quality, these values are instead determined based on empirical data. The modified creep index, μ^*, and the lateral earth pressure at rest for normally consolidated state, K_0^{NC}, are also set based on empiricism. The OCR, however, is based on collected data from the site.

The value of Poisson's ratio for unloading-reloading, ν'_{ur}, is assumed to be 0.2. It should be mentioned that the value for ν'_{ur} and the value for Poisson's ratio in the MC model, ν', in actuality should not be the same (Karstunen & Amavasai, 2017). This is because the Poisson's ratio used in the MC model should compensate for the fact that the model is linearly elastic until failure, and therefore be much larger than its unloading-reloading counterpart. However, for the sake of simplicity, they are in this project assumed to be equal.

4.3.4 Creep-SCLAY1S

For the Creep-SCLAY1S model, the same values as in the Soft Soil Creep model are used for κ^*, ν'_{ur}, OCR, and K_0^{NC}. The modified intrinsic compression index, λ_i^*, and the initial void ratio, e_0, are assumed based on empirical values. The modified intrinsic creep index, μ_i^*, is assumed to be the same as μ^*. The critical state stress ratio in compression and extension, M_c and M_e respectively, are calculated based on the friction angle by using Equation 4.1 (Muir Wood, 1991).

$$M_c = \frac{6\ sin(\varphi')}{3 - sin(\varphi')} \qquad M_e = \frac{6\ sin(\varphi')}{3 + sin(\varphi')} \tag{4.1}$$

The initial amount of bonding, χ_0, can be determined based on the sensitivity, S_t, by using Equation 4.2.

$$\chi_0 = S_t - 1 \tag{4.2}$$

The sensitivity of the clay at Nolhaga is derived from the previous site investigations. Equation 4.2 above is then used to calculate the initial amount of bonding in the model. Plaxis requires the input of interface parameters when using the Creep-SCLAY1S model. When it comes to these parameters, the cohesion, friction angle, and oedometer modulus are assumed to be the same as the cohesion, friction angle, and Young's modulus in the Mohr-Coulomb model.

Due to lack of relevant data from the site, the remaining Creep-SCLAY1S parameters are assumed based on empirical values.

4.4 Meshing

Six-noded elements are used to generate the meshes for the analysed slope sections. The fineness of the meshes are balanced to get an acceptable mesh quality while keeping down the calculation times. The final meshes can be seen in Appendix D.

4.5 Calculation stages

River formation phases are performed prior to adding the new building loads. This is done in order to achieve more realistic initial principal stresses in the soil. The way the process has been modelled is based on the work by Sellin (2023). The models are initialized with completely horizontal geometry and water table. Soil is then gradually removed over time, together with a lowering of the water table to form the river. The pond in section E is formed the same way. Since it is impossible to know how long this process took in reality, an arbitrary time span of 1000 years is chosen, with a fifth of the soil being removed every 200 years. This gives enough time for all the developed excess pore pressures to dissipate. The displacements are then reset to zero, so that the geometry corresponds to what has currently been measured at the site.

After the river formation phases are completed, the building loads are added, and phases simulating bank erosion are performed. The erosion phases are split up into 50-year intervals where soil is gradually removed, with thicknesses corresponding to Table 4.1. In order to analyze the influence of erosion on the expected displacements and safety factors, calculations are also performed where no soil is removed during the erosion phases. Instead, the model is allowed to consolidate for the 400 year time period, without any change in the geometry.

Safety factor calculations are performed for the MC and SSC models using *phi/c reduction*. This is done for each erosion phase, and for the initial conditions (IC), where the river has formed but no loads have been added, as well as after construction (AC), where the loads have been added but erosion has yet to take place.

No safety factors can be calculated when using the Creep-SCLAY1S model, as this model does not take φ' or c' as input.

See Table 4.2 for a summary of all the calculation phases in the Plaxis models, with their corresponding calculation type and time span.

Table 4.2: Table showing all calculation phases in the Plaxis models. For the Creep-SCLAY1S models, the safety calculations are not run.

Phase nr.	**Description**	**Calculation type**	**Time (days)**
0	Initial phase	K0 procedure	-
1	River formation 200 years	Consolidation	73 000
2	River formation 400 years	Consolidation	73 000
3	River formation 600 years	Consolidation	73 000
4	River formation 800 years	Consolidation	73 000
5	River formation 1 000 years	Consolidation	73 000
6	SF initial conditions	Safety	-
7	Add construction	Consolidation	50
8	SF after construction	Safety	-
9	Erosion 50 years	Consolidation	18 250
10	SF erosion 50 years	Safety	-
11	Erosion 100 years	Consolidation	18 250
12	SF erosion 100 years	Safety	-
13	Erosion 150 years	Consolidation	18 250
14	SF erosion 150 years	Safety	-
15	Erosion 200 years	Consolidation	18 250
16	SF erosion 200 years	Safety	-
17	Erosion 250 years	Consolidation	18 250
18	SF erosion 250 years	Safety	-
19	Erosion 300 years	Consolidation	18 250
20	SF erosion 300 years	Safety	-
21	Erosion 350 years	Consolidation	18 250
22	SF erosion 350 years	Safety	-
23	Erosion 400 years	Consolidation	18 250
24	SF erosion 400 years	Safety	-

5

Results and discussion

The following chapter presents and discusses the findings of the performed analyses. Data on both the vertical and horizontal displacements, as well as the development of excess pore water pressures below the buildings, are collected from the numerical models. The post-processing locations can be seen in Appendix E.

5.1 Serviceability

This chapter presents the calculated vertical and horizontal displacements, which are tied to the serviceability of the infrastructure at the site.

5.1.1 Vertical displacements

Example graphs of the vertical displacements developing with time for sections A and E with each constitutive model can be seen in Figure 5.1. The vertical displacement for the rest of the sections are presented in Appendix F. For all sections the Mohr-Coulomb model predicts the lowest total settlements, and Creep-SCLAY1S predicts the highest. The reason for this is likely because of the fact that the MC model is linear elastic until failure, and therefore does not develop as large plastic strains as the other two models. The fact that the Creep-SCLAY1S model predicts higher settlements than the SSC model is thought to have to do with the differences in how the models calculate creep, as mentioned in Chapter 2.2.4. The fact that Creep-SCLAY1S takes destructuration into account is also seen as a possible contributing factor.

Something worth noting is that the SSC model predicts the highest settlements between the 50- to 250-year time steps in section E, see Figure 5.1. A tendency toward the same behaviour can also be seen in section D. This is believed to have to do with the sand layer that is present at the bottom of these two sections. The higher permeability of this layer leads to a more open bottom boundary, compared to the other sections, which in turn speeds up the consolidation process. This can also be observed in the dissipation of excess pore water pressures. Graphs over the development of excess pore water pressure with time for sections A and E can be seen in Figure 5.2, with the other sections available in Appendix G. Here, both the MC and SSC models predict higher rates of dissipation in section E compared to

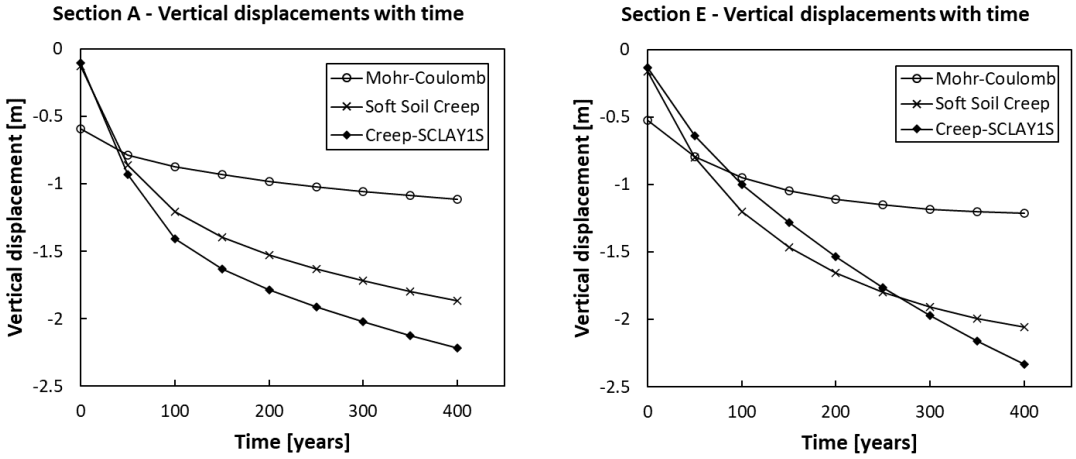

Figure 5.1: Vertical displacement development over time for sections A and E using different constitutive models.

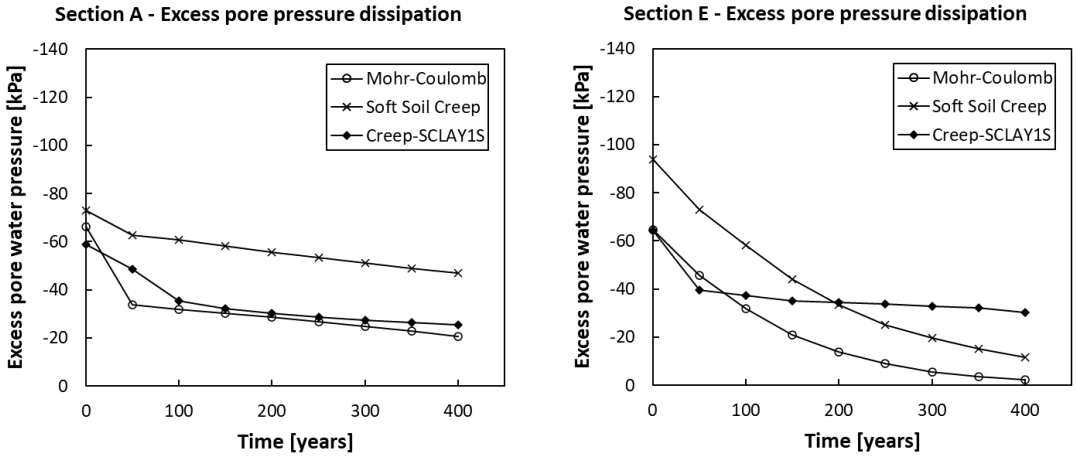

Figure 5.2: Excess pore water pressure dissipation over time for sections A and E using different constitutive models.

the other sections, whereas the Creep-SCLAY1S model seems to remain relatively unchanged. This means that the models will behave quite differently depending on whether the bottom groundwater flow boundary condition is open or closed. Therefore, it is very important to establish where the actual bedrock surface lies at the site, since it may severely affect the predicted movements. Overall, it can be concluded that the largest settlements are developing in sections A, C, and E for all three constitutive models, whereas section B is predicted to experience the smallest settlements.

5.1.2 Horizontal displacements

Example graphs over the horizontal displacement profile with depth to the right of the building in section E with the different constitutive models can be seen in Figure 5.3. Graphs over the horizontal displacement profiles for the rest of the locations and sections are presented in Appendix H. The MC and Creep-SCLAY1S models generally predict higher horizontal displacements than the SSC model. This is interesting, since the MC model estimates smaller vertical displacements than SSC for all sections. However, the depth where the largest horizontal displacements occur differs between MC and the other two models. With the MC model, the largest displacements tend to develop deeper down in the soil. In contrast, with SSC and Creep-SCLAY1S the largest displacements appear closer to the surface, tied to the first occurrences of clay layers. This is believed to have to do with MC over-predicting heave, where the riverbed is estimated to be pushed up much more as a result of unloading due to the erosion, compared with the other two models. This in turn causes higher displacements deeper in the soil that is closer to the riverbed.

When comparing the two creep models, it can be seen that Creep-SCLAY1S estimates that the soil overall shifts closer to the river (to the right in the graphs), compared to the SSC model. Just as with their differences in vertical displacements, this is likely due to how these models calculate creep, as well as the additional parameters that Creep-SCLAY1S takes into account, namely the anisotropy of the clay. Overall, as with the settlements, the highest horizontal displacements occur in sections A, C, and E.

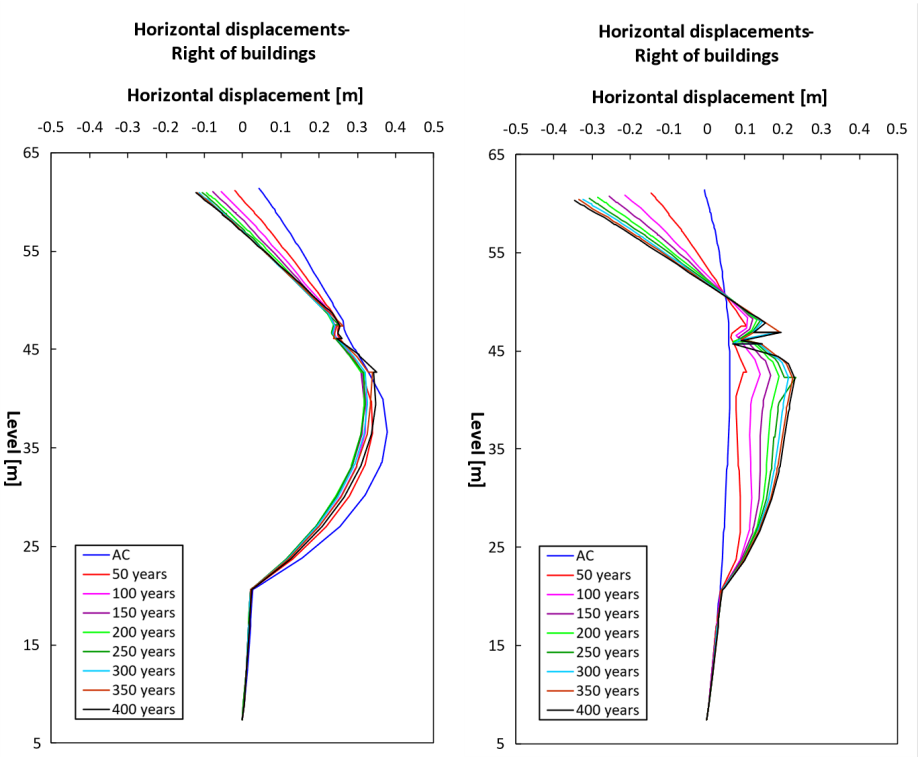

(a) Mohr-Coulomb

(b) Soft Soil Creep

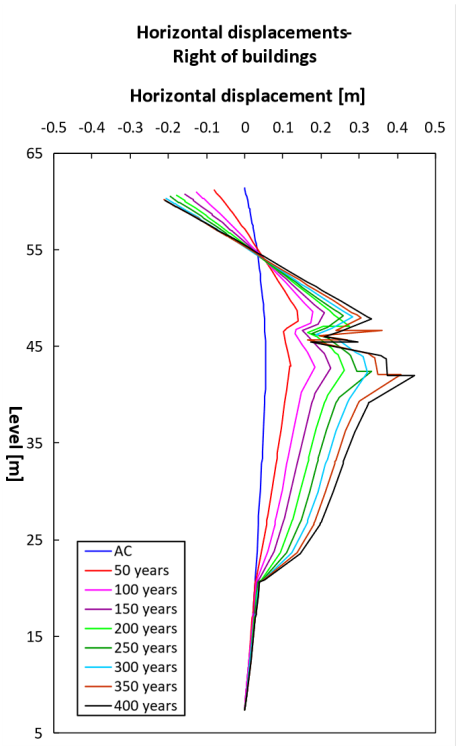

(c) Creep-SCLAY1S

Figure 5.3: Section E horizontal displacements in the right cross section with the different constitutive models.

5.2 Stability

The calculated safety factors over time using *phi/c reduction* in Plaxis from the MC and SSC models for each section are presented in Figure 5.4. As stated in Chapter 4.5, no safety factors can be calculated for Creep-SCLAY1S, as this model does not take φ' or c' as input. The reason why simulations for all time steps are not present in the MC and SSC calculations of section D is that the slope in this section fails after 100 years for MC, and after 150 years for SSC. This means that further calculations have to be aborted, and only the results prior to these time steps are available.

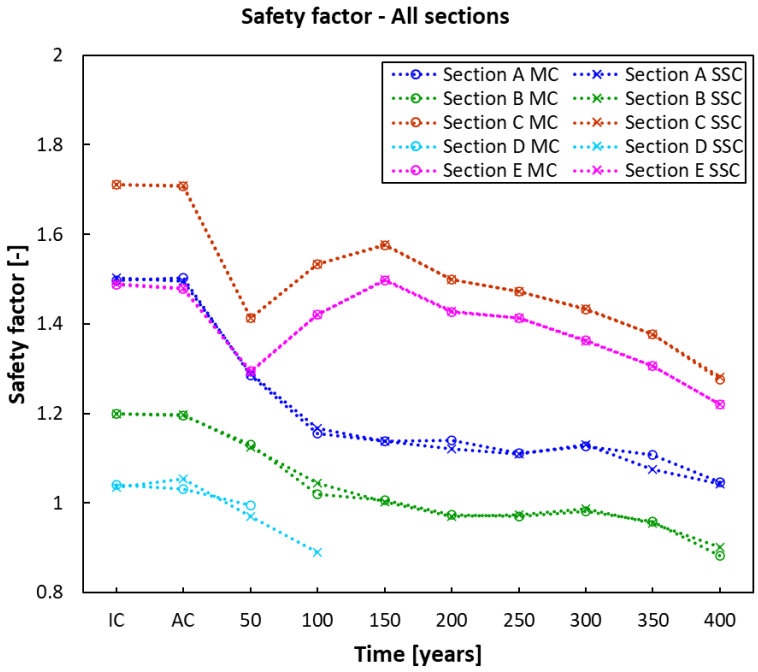

Figure 5.4: Development of safety factors over time for all sections. IC and AC on the time-axis stand for "initial conditions" and "after construction" respectively. These two phases are not in scale with the rest of the time steps.

Overall, there is a decrease in safety factor with time for all sections. However, for sections C and E, a temporary increase can be seen for the 100 year and 150 year time steps. This likely occurs due to a combination of the shape of the slopes in those sections, and how erosion has been modelled in Plaxis. This leads to a temporary decrease in slope steepness for these sections when removing material during the mentioned time steps. The conclusion can thus be drawn that slope inclination is a highly sensitive parameter when estimating the safety factor for the studied sections. A suggestion to deal with this issue would be to perform an erosion study of the riverbanks near Nolhaga in order to get a better view of the actual erosion patterns, thereby ensuring more accurate slope inclination developments. Another alternative would be to conduct a fully probabilistic analysis of the slope stability and include the potential variations in the erosion pattern. In that way, the uncertainties involved can be better understood, and a more informed decision can

be made on whether potential remedial actions, such as installing erosion protection, are necessary.

A further observation is that the safety factor drops quite drastically after the first erosion step in sections A, C, and E. This is believed to be because of a large increase in slope steepness from the erosion, together with the building loads subsequently getting closer to the bank.

When it comes to risk of slope failure, the safety factor is predicted to drop below 1 for two of the analysed sections, namely sections B and D. The safety factor in section B is estimated to decrease below 1 after approximately 200 years. This is believed to be caused by a combination of an increase in slope inclination, a heightening of the slope due to a lowering of the riverbed, and the bank getting closer to the building loads. The safety factor in section D drops below 1 already after 50 years, which is seen as reasonable, since the safety factor is already very close to 1 during the initial conditions. Since section D has the lowest initial safety factor, it is assumed to be the most critical slope from a stability perspective. This is in agreement with the conclusions drawn by the previous geotechnical investigations of the site, which also determined the slope in section D to be the most critical.

It can be seen that the calculated safety factor for both the MC and SSC models are the same in all sections for most time steps, even though the predicted displacements with these models differ significantly. This is speculated to have to do with how *phi/c reduction* works in Plaxis, which in practice seems to reduce the behaviour of SSC to that of the MC model.

5.3 Effect of erosion

As mentioned in Chapter 4.5, simulations with no erosion are run for all sections and constitutive models. The difference in displacements between the erosion and non-erosion scenario is then calculated. This difference is then divided by the estimated displacements in the scenario with erosion. In this way, the contribution of erosion to the overall displacements can be evaluated. This is done for both the vertical and horizontal displacements. The changes in vertical and horizontal displacements for sections C and E can be seen in Figure 5.5 and 5.6. The results for the rest of the sections are presented in Appendix I.

Overall, the factors are positive, meaning that the displacements are larger in the scenario with erosion. The differences also increase with time. This is deemed as reasonable, since the slopes get more and more eroded as time goes on, which will lead to larger displacements compared to the non-erosion scenario where the slopes remain unchanged. When it comes the variation between the models, SSC and Creep-SCLAY1S seem to produce quite similar results, see Figures 5.5 and 5.6. For the MC model, however, the expected increase in displacements due to erosion is significantly higher. This is believed to be related to the overestimation of heave by the model, where the unloading that occurs when removing soil during erosion

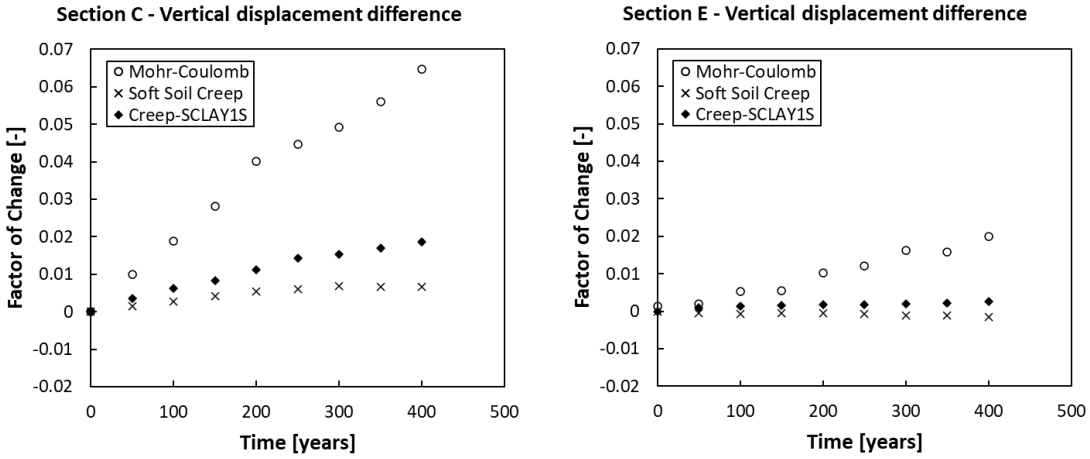

Figure 5.5: Change in vertical displacements in sections C and E as a result of modelling erosion.

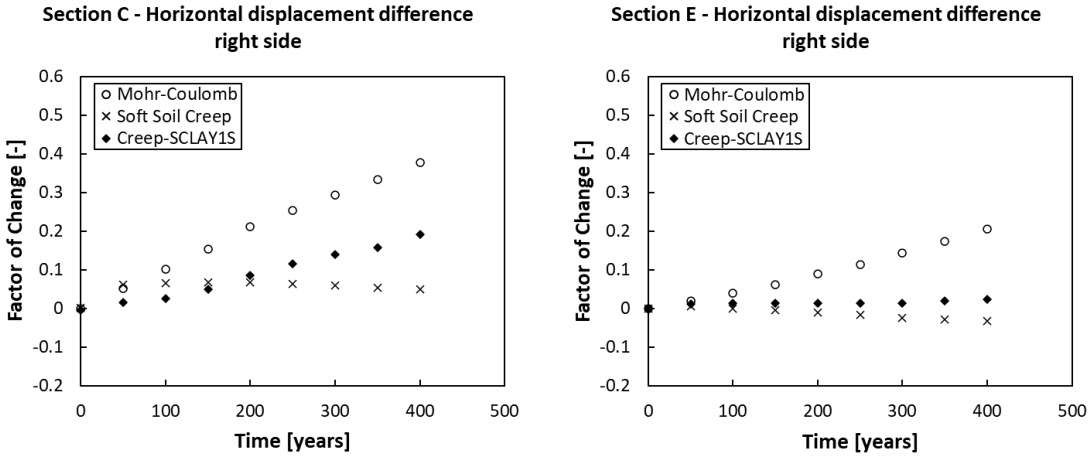

Figure 5.6: Change in horizontal displacements in sections C and E as a result of modelling erosion.

creates a much stronger response in the MC model, which in turn causes larger differences in the erosion versus non-erosion scenarios.

The erosion does not seem to significantly impact the magnitude of expected vertical displacements, with at most about 2% being due to erosion for the SSC and Creep-SCLAY1S models, and up to 6.5% for the MC model. The horizontal displacements, however, seem to be more affected. For the cross sections to the right of the buildings, closest to the river, the increase due to erosion comes up to around 40% in sections A and C, and 50% in section B when using the MC model. For SSC and Creep-SCLAY1S, the largest increase is in section A, and comes up to about 30%.

Without erosion, the estimated safety factors do not decrease at all, and stays on the same value as in the initial conditions. Thus, the slopes are predicted to become less stable solely due to the effects of erosion.

5.4 Impact on infrastructure

As a result of the settlements in sections A, C, and E, incremental deviatoric strains can be seen increasing with time below the buildings when using the Creep-SCLAY1S model, see Figure 5.7 for an example from section C, with the other two sections available in Appendix J. This is usually a sign of a developing failure plane, and the shapes resemble the ones seen in the classical bearing capacity failure case. It could

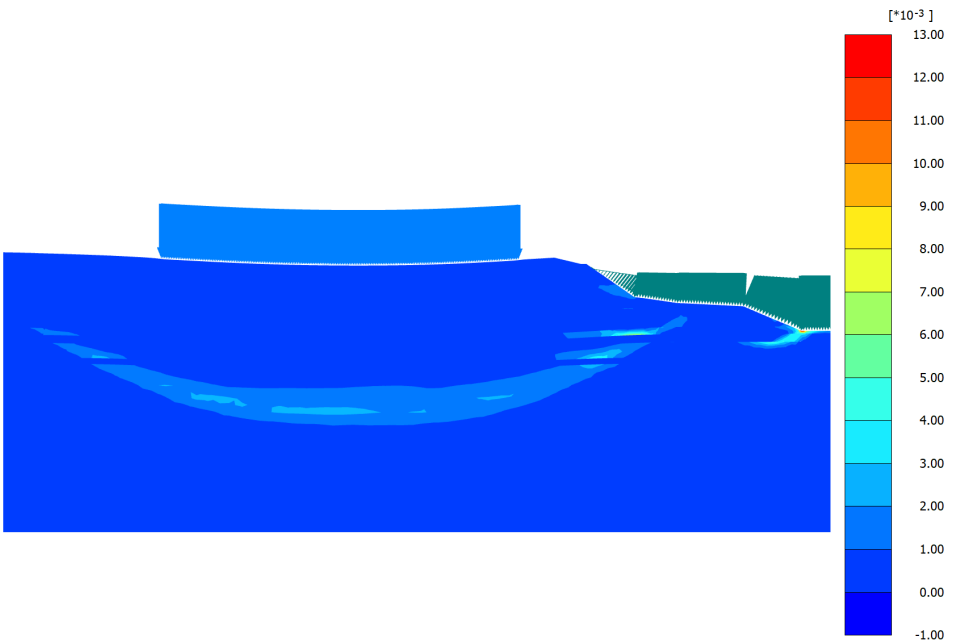

Figure 5.7: Section profile showing the locations of the developing incremental deviatoric strains after 400 years using the Creep-SCLAY1S model in section C.

therefore lead to large impacts on the infrastructure located in these sections. When plotting the incremental deviatoric strains against logged time, a sharp increase can be seen for all three sections, see Figure 5.8. However, the strains in sections C and E seem to decrease after some time. Additionally, there does not seem to be any increases in excess pore water pressures in any of the sections, which would otherwise also point toward a developing failure plane. Furthermore, these strain increases only start appearing after about 300-400 years, which is a considerable amount of time. Despite this, the developing strains are still seen as a potential issue, and are therefore reported in this assessment.

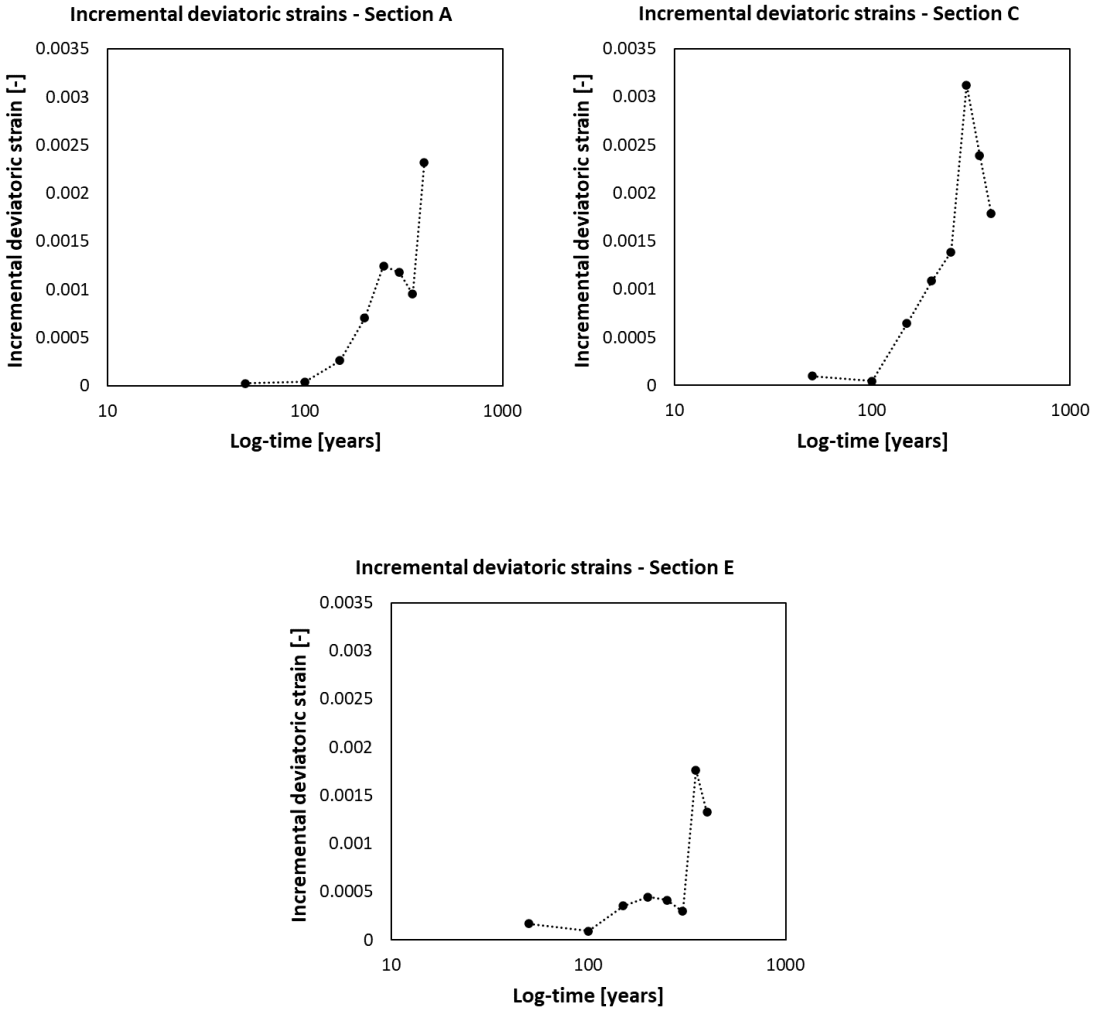

Figure 5.8: Incremental deviatoric strains with time below the middle of the building at approximately +37 m, using Creep-SCLAY1S, in sections A, C, and E.

Additionally, the estimated vertical and horizontal displacements at the site risk affecting underground utilities such as wastewater pipes going in to the treatment plant. The lifespan for these pipes are according to the plan details approximately 100 years, and so only the calculated displacements within this time period are

relevant to investigate. Based on maps of planned underground utility placement, sections B, C, and E will have pipes that cross both left and right of the buildings, approximately where the measurements of horizontal displacements have been taken, see Figure 5.9. The pipes run at a level of around +58 (RH2000). The locations of the pipelines in each section, as well as graphs of the vertical and horizontal displacements over time in these points, are presented in Appendix K.

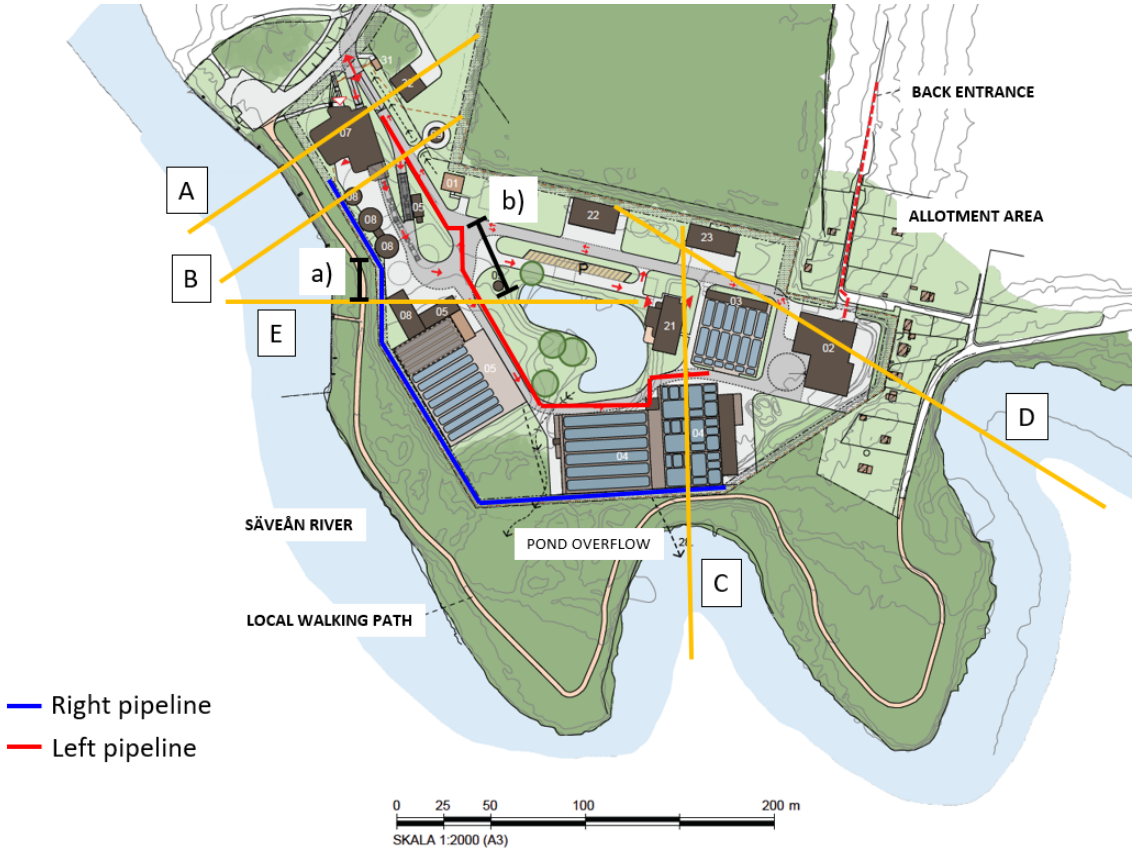

Figure 5.9: Map over the location of the analysed pipelines relative to the studied slope sections. Note that the pipelines are named left and right in relation to which side of the building they are in the section profiles, not on the map.

Previously performed pipe tolerance assessments are analysed in order to determine whether or not the calculated displacements risk damaging the pipes, see European Committee for Standardization (2007), Faeli et al. (2010), Wols et al. (2014), and Feng et al. (2020). Generally, relationships between the pipe diameter, D, and displacement are suggested. The value for the largest allowable differential displacement range between 0.1D to 0.15D in the analysed studies. Similar relationships are suggested between the pipe diameter and the minimum pipe length over which the differential displacements are allowed take place. These range between 10.5D to 35D. In order to more easily assess whether the calculated pipe displacements exceed these guidelines, without having to involve a pipe diameter, a ratio of the maximum allowable displacement over the minimum allowable pipe length is instead derived. This ratio then ranges between approximately 0.003 and 0.01, where a value located above this range would indicate a higher risk of pipe damage,

and a value below would indicate a lower risk. If the calculated value is within this range, it is seen as a potential for higher risk of pipe damage.

Since only a few 2D cross sections are analysed in this thesis, the lengths over which the estimated displacements take place are difficult to assess. However, based on the plan map over the area, and the locations of the calculated displacements relative to the pipelines, a possible critical length for each pipeline is identified. The lengths have been marked out as *a)* and *b)* in Figure 5.9. For both these pipeline groups, the differences in displacements between the two nearest sections, section B and E, are calculated and then divided by the assumed length, which is about 20 m for *a)* and 45 m for *b)*. The results can be seen in Tables 5.1-5.3, where the cells marked green indicate a low risk, cells marked yellow indicate a potential higher risk, and cells marked red indicate a higher risk of pipe damage.

Table 5.1: Ratio between calculated vertical and horizontal displacements, and assumed pipeline length when using the Mohr-Coulomb model.

Mohr-Coulomb	Left pipelines		Right pipelines	
Years	50	100	50	100
Vertical displacement ratio	0.0033	0.0047	0.0007	0.0048
Horizontal displacement ratio	0.0030	0.0024	0.0018	0.0011

Table 5.2: Ratio between calculated vertical and horizontal displacements, and assumed pipeline length when using the Soft Soil Creep model.

Soft Soil Creep	Left pipelines		Right pipelines	
Years	50	100	50	100
Vertical displacement ratio	0.0031	0.0053	0.0034	0.0026
Horizontal displacement ratio	0.0009	0.0022	0.0013	0.0027

Table 5.3: Ratio between calculated vertical and horizontal displacements, and assumed pipeline length when using the Creep-SCLAY1S model.

Creep-SCLAY1S	Left pipelines		Right pipelines	
Years	50	100	50	100
Vertical displacement ratio	0.0027	0.0043	0.0155	0.0117
Horizontal displacement ratio	0.0021	0.0015	0.0042	0.0063

It can be seen that the results differ between the constitutive models, where the highest overall risks for damage are predicted in the pipelines to the right of the buildings when using the Creep-SCLAY1S model. However, for the MC and SSC models, the highest risks are related to the pipelines on the left. The vertical displacements seem to be the largest issue for all models, which is to be expected since the magnitude of these displacements are much larger than the horizontal ones.

Based on these calculations, it can be concluded that both of the pipeline groups are at risk of being damaged by the calculated displacements.

In order to assess the impact that the erosion has on these risks, the ratios were also calculated using the calculated displacements in the non-erosion scenario. These results can be seen in Tables 5.4-5.6.

Table 5.4: Ratio between calculated vertical and horizontal displacements in the non-erosion scenario, and assumed pipeline length when using the Mohr-Coulomb model.

Mohr-Coulomb - No erosion	Left pipelines		Right pipelines	
Years	50	100	50	100
Vertical displacement ratio	0.0033	0.0047	0.0008	0.0049
Horizontal displacement ratio	0.0028	0.0020	0.0018	0.0010

Table 5.5: Ratio between calculated vertical and horizontal displacements in the non-erosion scenario, and assumed pipeline length when using the Soft Soil Creep model.

Soft Soil Creep - No erosion	Left pipelines		Right pipelines	
Years	50	100	50	100
Vertical displacement ratio	0.0031	0.0053	0.0034	0.0025
Horizontal displacement ratio	0.0009	0.0022	0.0012	0.0027

Table 5.6: Ratio between calculated vertical and horizontal displacements in the non-erosion scenario, and assumed pipeline length when using the Creep-SCLAY1S model.

Creep-SCLAY1S - No erosion	Left pipelines		Right pipelines	
Years	50	100	50	100
Vertical displacement ratio	0.0027	0.0043	0.0154	0.0116
Horizontal displacement ratio	0.0020	0.0014	0.0041	0.0061

Here, a very slight decrease in some ratios can be seen. There are also a few ratios that increase. This is believed to be due to the influence of erosion on the displacements differing between the sections. This, in turn, means that the differences in the displacements have the possibility to decrease between some sections when implementing erosion. However, the overall risks are still similar. The only exception being the horizontal displacements after 50 years at the left pipeline when using the MC model. When excluding erosion, these displacements are seen as having a low risk of damaging the pipeline, whereas when erosion is included, the pipeline has a potentially higher risk of being damaged. Despite this, the conclusion can be drawn that erosion does not seem to influence which pipelines that are regarded as being at risk of damage from the calculated displacements in any meaningful way.

However, due to the lack of relevant site data, many assumptions have been made during the course of this project, both in terms of soil properties and modelled erosion. Because of this, there are large uncertainties associated with the presented results. Additionally, since no ground improvements measures have been included in the analysed models, the actual displacements at the site may differ significantly. This means that the calculated risk areas may change, and the influence of erosion may be higher or lower, depending on the conditions at the site. Therefore, it is recommended that further investigations are conducted to more accurately assess these risks, and ensure that necessary precautions are taken to protect the treatment plant from future issues related to these aspects.

6

Conclusions and recommendations

This chapter presents the conclusions drawn from the acquired results, as well as recommendations for further work based on these conclusions.

6.1 Conclusions

This thesis investigates the effects of riverbank erosion on the stability of nearby infrastructure by using data from a specific case study area. The investigation is done using three different constitutive soil models with increasing complexity: Mohr-Coulomb, Soft Soil Creep, and Creep-SCLAY1S. The differences in the expected displacements and safety factors between these models are then analysed.

The results show that Creep-SCLAY1S generally predicts the largest total vertical and horizontal displacements within the studied time period. The Soft Soil Creep model predicts the second largest vertical displacements, which is mainly thought to be related to the differences in the way that these two models predict creep. The Mohr-Coulomb model generally predicts the second largest horizontal displacements. This is believed to be related to the over-prediction of heave in the Mohr-Coulomb model, which seems to give increased horizontal displacements compared to the Soft Soil Creep model.

The calculated safety factors decrease with time as a direct consequence of the inflicted bank erosion. Two of the analysed slope sections are predicted to drop below a safety factor of 1 within the studied time period, which indicates a risk of failure: one after 50 years, and one after 200 years. There is no difference between the calculated safety factor in the Mohr-Coulomb model and the Soft Soil Creep model. This is believed to be related to how the safety factor is calculated in the used software.

The erosion of the riverbanks increases the expected vertical displacements by between 0-6.5%, with Mohr-Coulomb predicting the highest differences. The horizontal displacements are generally more affected by the erosion, and are at most estimated to increase by 30% with the Soft Soil Creep and Creep-SCLAY1S models, and by up to 50% when using Mohr-Coulomb.

The calculated displacements are at risk of damaging pipes related to the wastew-

ater plant, but the influence of erosion on these risks are deemed to be negligible. However, due to a lack of relevant site data many assumptions are made during this thesis. This means that the uncertainties regarding the exact locations and magnitudes of these displacements, and the exact influence of erosion, are very large. Therefore, it is recommended that further studies are made to gather more relevant data, and thus decrease the uncertainties in the results.

6.2 Recommendations

Proposed recommendations for further work are listed below:

- Perform an erosion study on the riverbanks at the site in order to get a better idea of the erosion rate and patterns in the area.
- If possible, perform additional testing, both *in-situ* and lab tests, in order to determine the material parameters used for the more advanced constitutive soil models.
- Conduct a fully probabilistic analysis to get a better idea of the uncertainties involved in the results.
- A 3D finite element analysis is recommended to get a better overview of the distance over which the displacements are expected to take place, and in that way be able to more accurately assess potential damage to infrastructure such as pipelines.
- Investigate how the effects of climate change may alter the erosion patterns at the site in the future, and how that in turn affects the infrastructure.

Bibliography

Bentley. (2023, December). PLAXIS 2D 2024.1: 2 - Reference Manual. https://bentleysystems.service-now.com/community?id=kb_article&sys_kb_id=082fe67a97668a1081d373b0f053afbc

Chassiot, L., Lajeunesse, P., & Bernier, J.-F. (2020). Riverbank erosion in cold environments: Review and outlook. *Earth-Science Reviews*, *207*, 103231. https://doi.org/10.1016/j.earscirev.2020.103231

Darby, S. E., Rinaldi, M., & Dapporto, S. (2007). Coupled simulations of fluvial erosion and mass wasting for cohesive river banks. *Journal of Geophysical Research: Earth Surface*, *112*(F3). https://doi.org/10.1029/2006JF000722

El Kadi Abderrezzak, K., Die Moran, A., Tassi, P., Ata, R., & Hervouet, J.-M. (2016). Modelling river bank erosion using a 2D depth-averaged numerical model of flow and non-cohesive, non-uniform sediment transport. *Advances in Water Resources*, *93*, 75–88. https://doi.org/10.1016/j.advwatres.2015.11.004

European Committee for Standardization. (2007, February). *EN 1993-4-3: Eurocode 3: Design of steel structures - Part 4-3: Pipelines* (tech. rep.). Brussels.

Faeli, Z., Fakher, A., & Sadatieh, S. (2010). Allowable Differential Settlement of Oil Pipelines. *International Journal of Engineering (IJE)*, *4*(4), 308–320. https://www.researchgate.net/publication/351929144

Feng, X., Li, H., Chen, B., Zhao, L., & Zhou, J. (2020). Numerical investigations into the failure mode of buried prestressed concrete cylinder pipes under differential settlement. *Engineering Failure Analysis*, *111*, 104492. https://doi.org/10.1016/j.engfailanal.2020.104492

Geotechdata.info. (2013, September). Soil Young's modulus. https://www.geotesting.org/parameter/soil-young-s-modulus

Google. (n.d.-a). [Google Earth photo over Nolhaga wastewater treatment plant]. https://earth.google.com/web/@57.93142295,12.50699391,61.62549966a,729.52342285d,30.00005537y,0h,0t,0r/data=MikKJwolCiExQ1FROW9oMm8zYUxzOGxLUD

Google. (n.d.-b). [Google maps photo over Alingsås]. https://maps.app.goo.gl/tzbkbg8DxTET2oBC6

Gras, J.-P., Sivasithamparam, N., Karstunen, M., & Dijkstra, J. (2017a). Permissible range of model parameters for natural fine-grained materials. *Acta Geotechnica*, *13*(2), 387–398. https://doi.org/10.1007/s11440-017-0553-1

Gras, J.-P., Sivasithamparam, N., Karstunen, M., & Dijkstra, J. (2017b). Strategy for consistent model parameter calibration for soft soils using multi-objective

optimisation. *Computers and Geotechnics*, *90*, 164–175. https://doi.org/10.1016/j.compgeo.2017.06.006

Hooke, J. M. (1979). An analysis of the processes of river bank erosion. *Journal of Hydrology*, *42*(1-2), 39–62. https://doi.org/10.1016/0022-1694(79)90005-2

Islam, A., & Guchhait, S. K. (2024). Riverbank Erosion: Basic Concepts and Approaches. In *Riverbank erosion in the bengal delta: An integrated perspective* (pp. 3–22). Springer International Publishing. https://doi.org/10.1007/978-3-031-47010-3{_}1

Jugie, M., Gob, F., Virmoux, C., Brunstein, D., Tamisier, V., Le Coeur, C., & Grancher, D. (2018). Characterizing and quantifying the discontinuous bank erosion of a small low energy river using Structure-from-Motion Photogrammetry and erosion pins. *Journal of Hydrology*, *563*, 418–434. https://doi.org/10.1016/j.jhydrol.2018.06.019

Kandalai, S., John, N. J., & Patel, A. (2023). Effects of Climate Change on Geotechnical Infrastructures — state of the art. *Environmental Science and Pollution Research*, *30*(7), 16878–16904. https://doi.org/10.1007/s11356-022-24788-7

Karstunen, M., & Amavasai, A. (2017, November). *BEST SOIL: Soft soil modelling and parameter determination* (tech. rep.). Chalmers University of Technology. Gothenburg.

Karstunen, M., Krenn, H., Wheeler, S. J., Koskinen, M., & Zentar, R. (2005). Effect of Anisotropy and Destructuration on the Behavior of Murro Test Embankment. *International Journal of Geomechanics*, *5*(2), 87–97. https://doi.org/10.1061/(ASCE)1532-3641(2005)5:2(87)

Larsson, R. (2008). *Jords egenskaper* (tech. rep.). Swedish Geotechnical Institute. Linköping. https://www.sgi.se/globalassets/publikationer/info/pdf/sgi-i1.pdf

Lawler, D. M. (1986). River Bank Erosion and the Influence of Frost: A Statistical Examination. *Transactions of the Institute of British Geographers*, *11*(2), 227. https://doi.org/10.2307/622008

Leoni, M., Karstunen, M., & Vermeer, P. A. (2008). Anisotropic creep model for soft soils. *Géotechnique*, *58*(3), 215–226. https://doi.org/10.1680/geot.2008.58.3.215

Luppi, L., Rinaldi, M., Teruggi, L. B., Darby, S. E., & Nardi, L. (2009). Monitoring and numerical modelling of riverbank erosion processes: a case study along the Cecina River (central Italy). *Earth Surface Processes and Landforms*, *34*(4), 530–546. https://doi.org/10.1002/esp.1754

Muir Wood, D. (1991, April). *Soil Behaviour and Critical State Soil Mechanics*. Cambridge University Press. https://doi.org/10.1017/CBO9781139878272

Muir Wood, D. (2004, December). *Geotechnical Modelling*. CRC Press. https://doi.org/10.1201/9781315273556

Roscoe, K. H., & Burland, J. B. (1968, March). On the generalized stress-strain behavior of "wet" clay. In J. Heyman & F. A. Leckie (Eds.), *Engineering plasticity* (pp. 535–609, Vol. 7). Cambridge University Press.

Saadon, A., Abdullah, J., Muhammad, N. S., Ariffin, J., & Julien, P. Y. (2021). Predictive models for the estimation of riverbank erosion rates. *CATENA*, *196*, 104917. https://doi.org/10.1016/j.catena.2020.104917

Sellin, C. (2023). *On modelling of slope stability in sensitive clay: the effect of time and state* [Doctoral dissertation, Chalmers University of Technology].

SGI. (2017). *Skredrisker i ett förändrat klimat – Säveån. Del 2: Metodik för kartläggning* (tech. rep.). Statens geotekniska institut, SGI Publikation 38–2. Linköping.

Sivasithamparam, N., Karstunen, M., & Bonnier, P. (2015). Modelling creep behaviour of anisotropic soft soils. *Computers and Geotechnics*, *69*, 46–57. https://doi.org/10.1016/j.compgeo.2015.04.015

Vermeer, P. A., & Neher, H. P. (1999). A soft soil model that accounts for creep. In *Beyond 2000 in computational geotechnics* (pp. 249–261). Routledge. https://doi.org/10.1201/9781315138206-24

Vermeer, P. A., Stolle, D. F. E., & Bonnier, P. G. (1998). From the classical theory of secondary compression to modern creep analysis. *Computer methods and advances in geomechanics*, 2469–2478. https://www.tib.eu/de/suchen/id/BLCP%3ACN026030054

Wheeler, S. J., Näätänen, A., Karstunen, M., & Lojander, M. (2003). An anisotropic elastoplastic model for soft clays. *Canadian Geotechnical Journal*, *40*(2), 403–418. https://doi.org/10.1139/t02-119

Wols, B., van Daal, K., & van Thienen, P. (2014). Effects of Climate Change on Drinking Water Distribution Network Integrity: Predicting Pipe Failure Resulting from Differential Soil Settlement. *Procedia Engineering*, *70*, 1726–1734. https://doi.org/10.1016/j.proeng.2014.02.190

A

Additional case study information

A.1 Sampling information

As part of the ground investigations performed before designing the new treatment plant, several boreholes were made. Ramboll investigated 15 boreholes distributed across the site. Prior to Ramboll, SWECO also did some ground investigations resulting in five additional boreholes. See Figure A.1 for a map over where the boreholes are located. The ones performed by SWECO are indexed by SW20XX and colored green, while the ones performed by Ramboll are indexed R20XX and colored blue and red.

Auger samples were gathered at all of the Ramboll boreholes. Piston samples and pore water pressure measurements were taken at R2001 and R2013, marked with red in Figure A.1. In terms of what tests that were performed, CPTs were carried out at all of the boreholes at the site. In the lab, the auger samples were analysed to determine soil type and water content. The piston samples were used to determine density, water content, and liquid limit at six different depth in the clay layer for both R2001 and R2013. Fall cone tests were also performed on these piston samples in order to determine sensitivity and undrained shear strength. CRS-tests were performed on piston samples for three different depths in the clay layer of both the sampled boreholes.

A.2 Location of new buildings

See figure A.2 for the plan map used in this project when determining the building loads.

Figure A.1: Map over borehole locations (Google, n.d.-a).

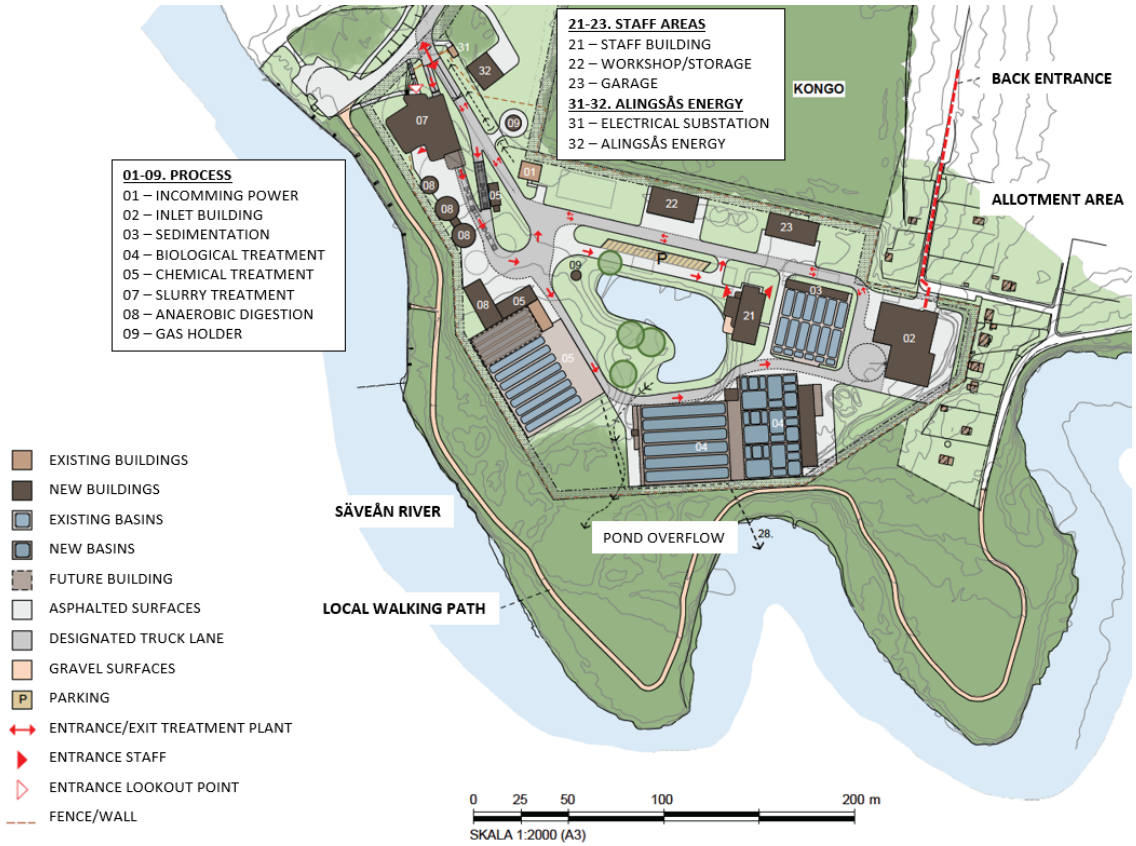

Figure A.2: Latest plan map over expected building placement at Nolhaga from Ramboll.

B

Numerical model dimensions

Figures B.1-B.5 below show simplified sketches containing model dimensions (not in scale). The exact shapes of the riverbeds are not included, instead only the channel width and depth are presented. For a more detailed look at the geometries used in the numerical modelling, see Appendix D.

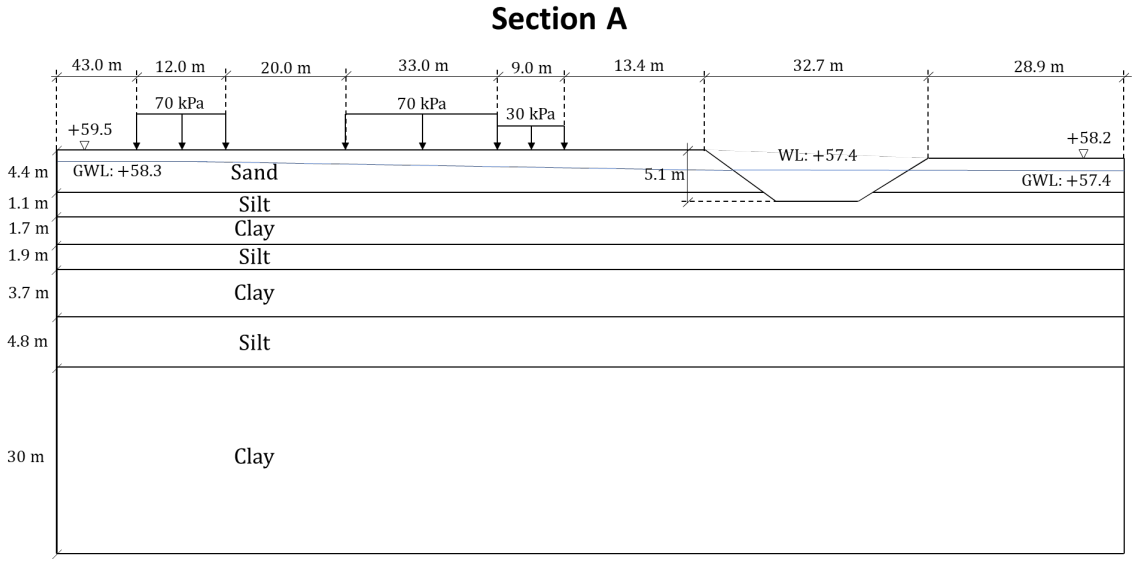

Figure B.1: Sketch showing the dimensions the section A model, including applied loads.

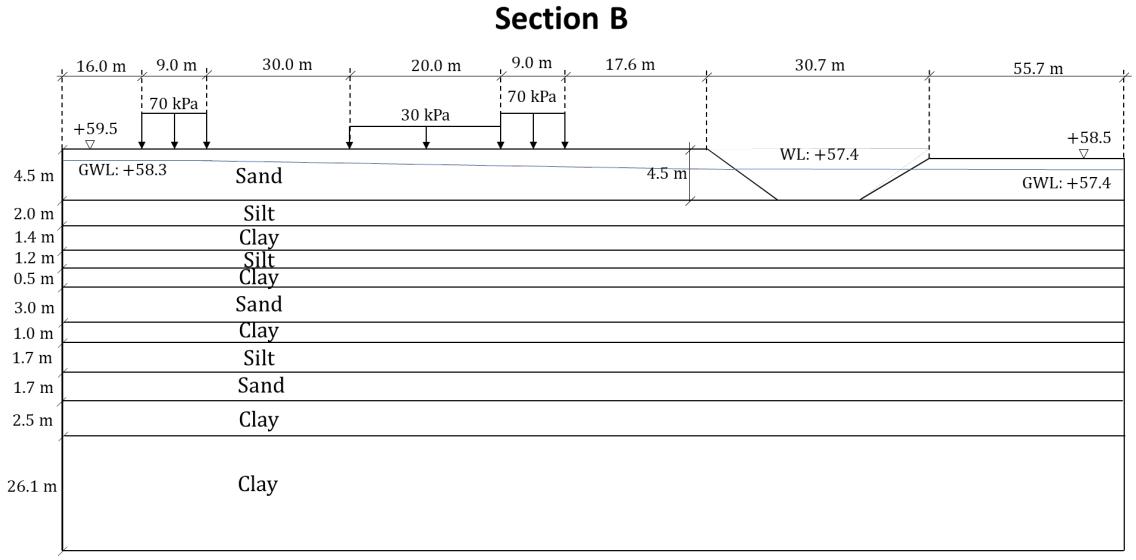

Figure B.2: Sketch showing the dimensions the section B model, including applied loads.

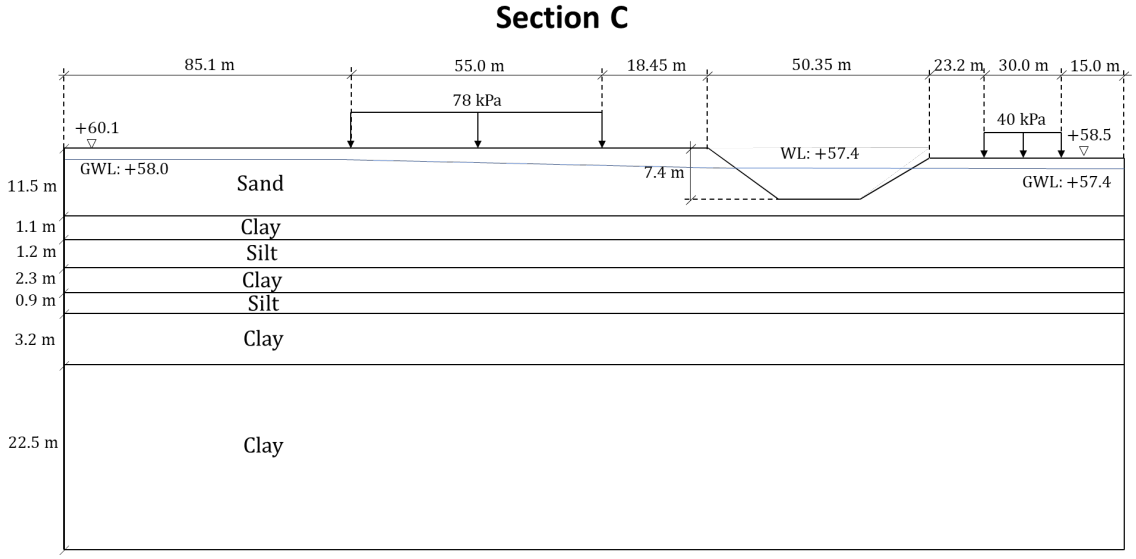

Figure B.3: Sketch showing the dimensions the section C model, including applied loads.

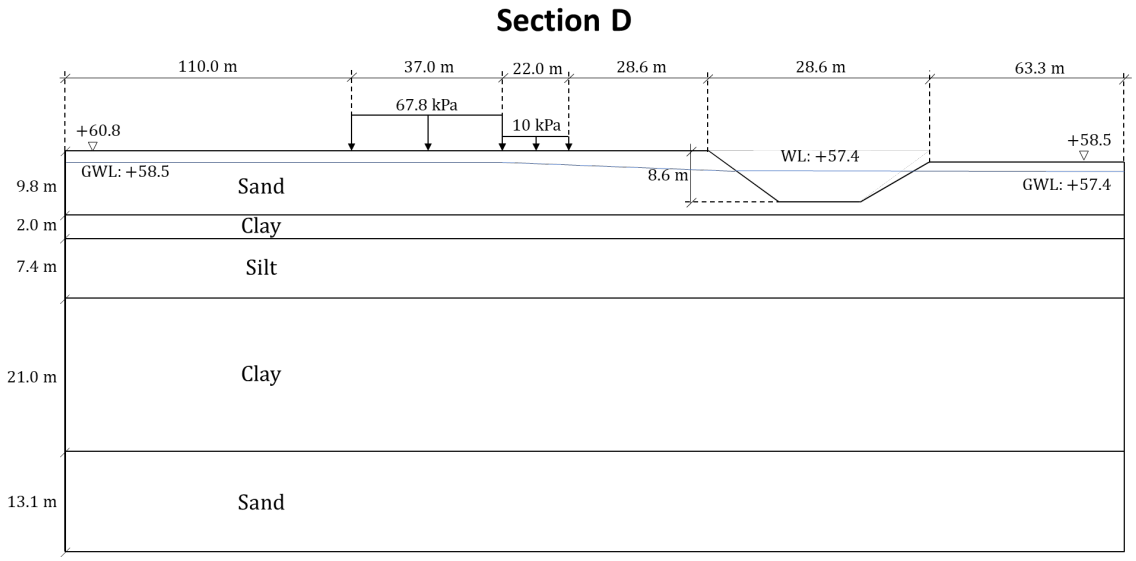

Figure B.4: Sketch showing the dimensions the section D model, including applied loads.

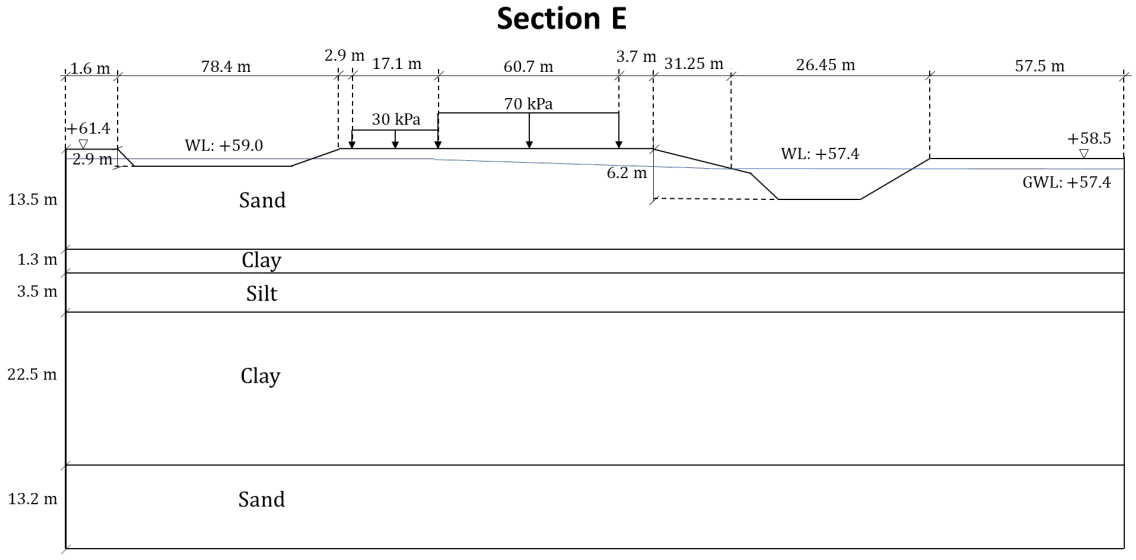

Figure B.5: Sketch showing the dimensions the section E model, including applied loads.

C

Constitutive soil model parameters

Table C.1: General parameter values used for all constitutive soil models.

Parameter	Description	Sand	Silt	Clay	Unit
γ_{unsat}	Unsaturated unit weight	10	9	8	kN/m^3
γ_{sat}	Saturated unit weight	18	17	18	kN/m^3
k	Permeability	10^{-4}	10^{-8}	10^{-10}	m/s

Table C.2: Parameter values used for the Mohr-Coulomb model.

Parameter	Description	Sand	Silt	Clay	Unit
E'_{ref}	Reference effective Young's modulus	15 000	10 000	1 000	kN/m^2
ν'	Poisson's ratio	0.2	0.2	0.2	-
c'_{ref}	Reference effective cohesion	1.5	1.0	3.3	kN/m^2
c_{inc}	Increase in cohesion with depth			0.21 (after 20 m)	$kN/m^2/m$
φ'	Friction angle	31.0	28.0	30.0	$^\circ$
$K_{0,x/z}$	Coefficient of lateral earth pressure at rest	0.4850	0.5305	0.6	-

Table C.3: Parameter values used for the Soft Soil Creep model.

Parameter	Description	Value	Unit
λ^*	Modified compression index	0.296	-
κ^*	Modified swelling index	0.020	-
μ^*	Modified creep index	0.0025	-
ν'_{ur}	Poisson's ratio for unloading-reloading	0.2	-
c'_{ref}	Reference effective cohesion	3.3	kN/m^2
φ'	Friction angle	30.0	°
K_0^{NC}	Coefficient of lateral earth pressure at rest under normally consolidated conditions	0.6	-
OCR	Overconsolidation ratio *in situ*	1.3	-

Table C.4: Parameter values used for the Creep-SCLAY1S model.

Parameter	Description	Value	Unit
κ^*	Modified swelling index	0.020	-
ν'_{ur}	Poisson's ratio for unloading-reloading	0.2	-
λ_i^*	Modified intrinsic compression index	0.108	-
M_c	Critical state stress ratio in compression	1.2	-
M_e	Critical state stress ratio in extension	0.86	-
ω	Absolute effectiveness of rotational hardening	30.0	-
ω_d	Relative effectiveness of rotational hardening	1.0	-
ζ	Absolute effectiveness of destructuration	9.0	-
ζ_d	Relative effectiveness of destructuration	0.4	-
OCR	Overconsolidation ratio *in situ*	1.3	-
e_0	Initial void ratio	2.0	-
α_0	Initial inclination of yield surface	0.63	-
χ_0	Initial amount of bonding	19.0	-
τ	Reference time	1	days
μ_i^*	Modified intrinsic creep index	0.0025	-
K_0^{NC}	Coefficient of lateral earth pressure at rest under normally consolidated conditions	0.6	-
E_{oed}^{ref}	Reference tangential oedometer modulus	1 000	kN/m^2
$c_{ref,inter}$	Reference interface cohesion	3.3	kN/m^2
φ_{inter}	Interface friction angle	30.0	°

D

Numerical model meshes

In the following numerical models, the soil layers are color-coded according to Figure D.1 below.

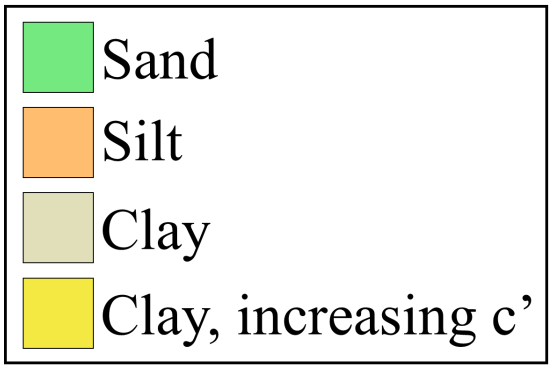

Figure D.1: Legend showing the colors of the different soil layers in the numerical models.

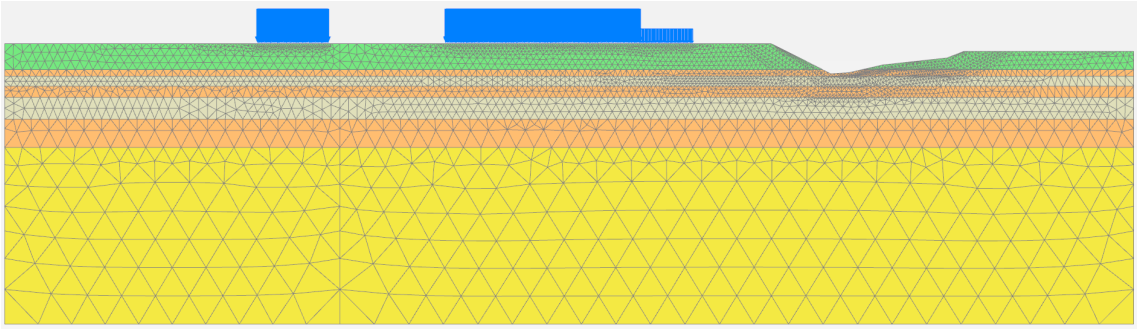

Figure D.2: Plaxis numerical model mesh for section A.

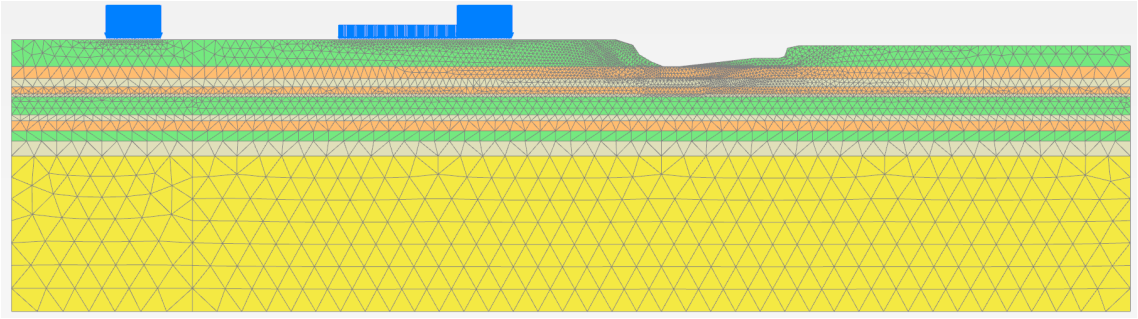

Figure D.3: Plaxis numerical model mesh for section B.

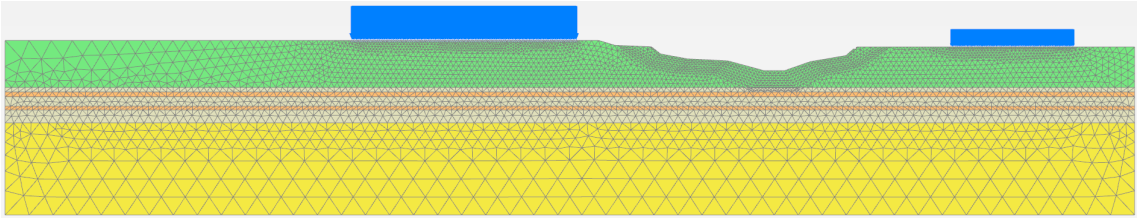

Figure D.4: Plaxis numerical model mesh for section C.

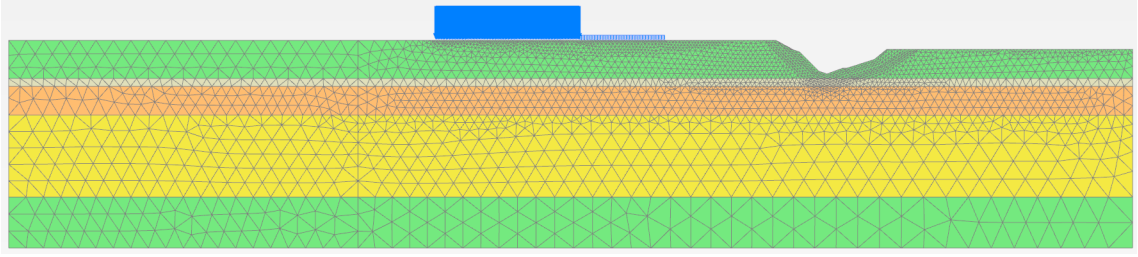

Figure D.5: Plaxis numerical model mesh for section D.

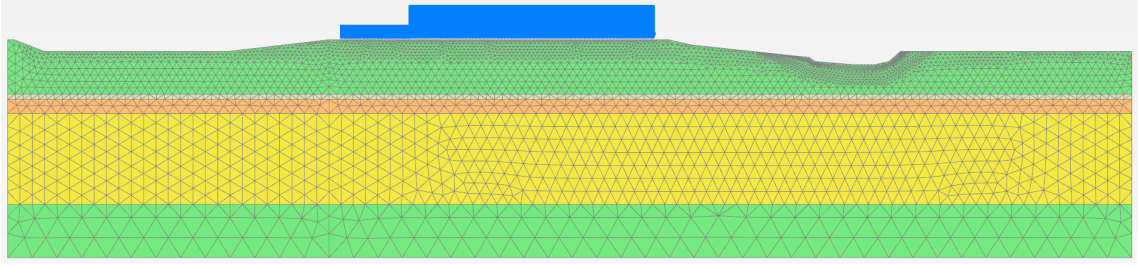

Figure D.6: Plaxis numerical model mesh for section E.

E

Post-processing locations

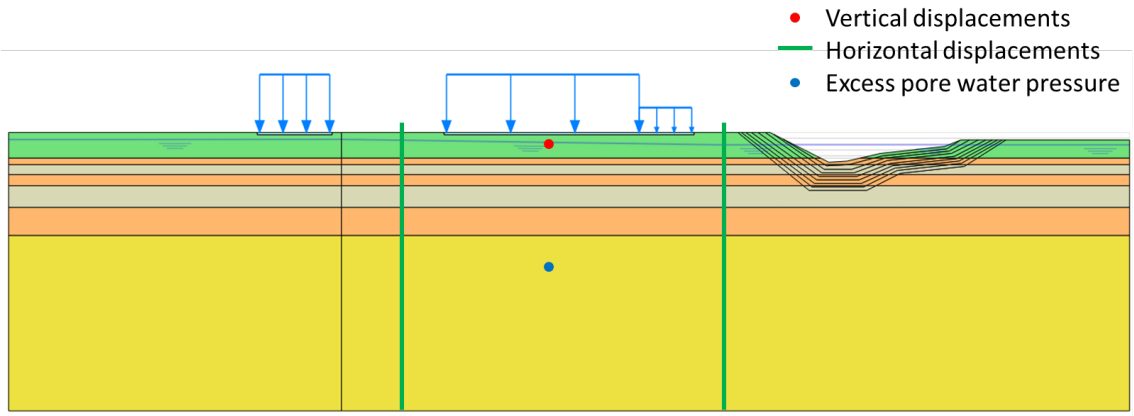

Figure E.1: Post-processing locations for section A.

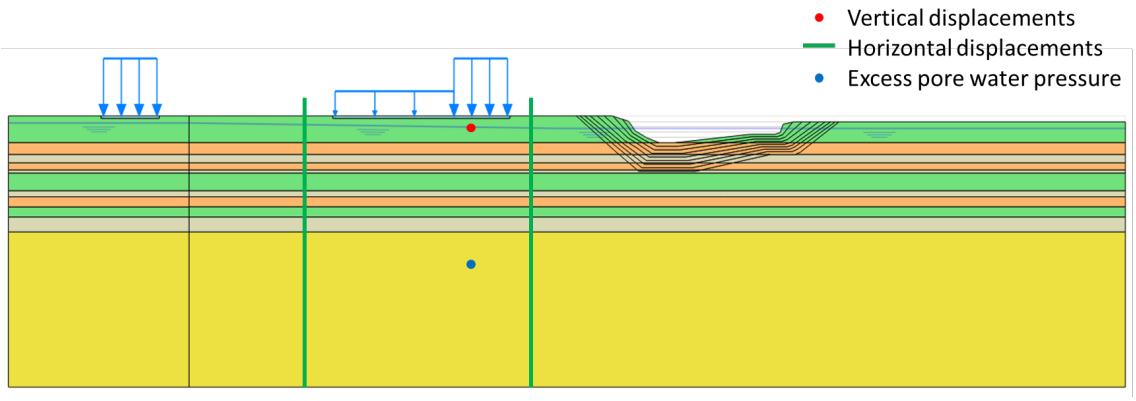

Figure E.2: Post-processing locations for section B.

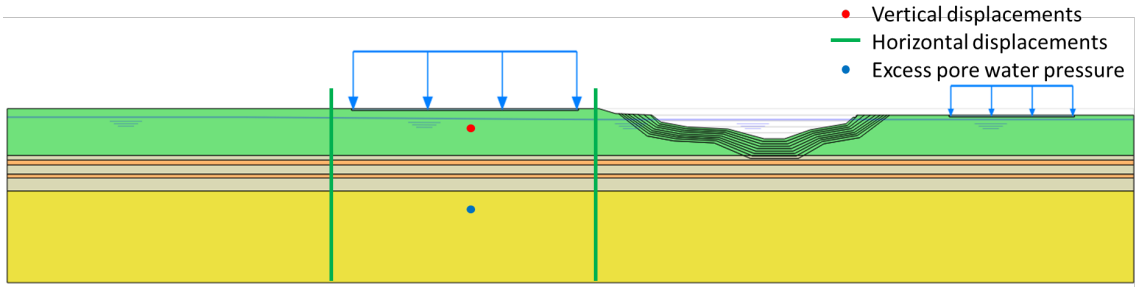

Figure E.3: Post-processing locations for section C.

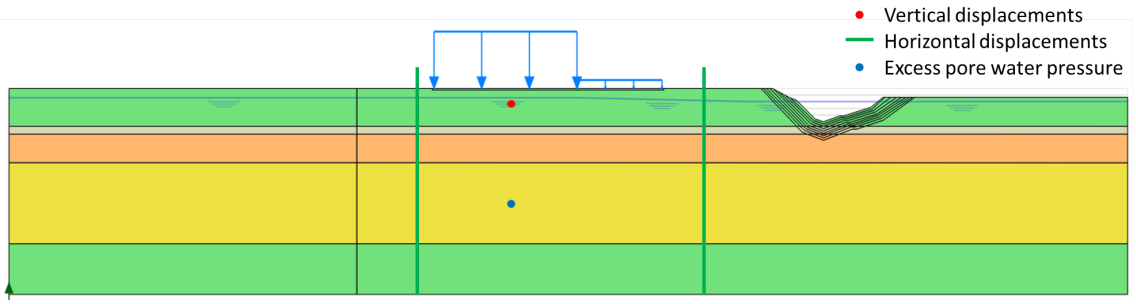

Figure E.4: Post-processing locations for section D.

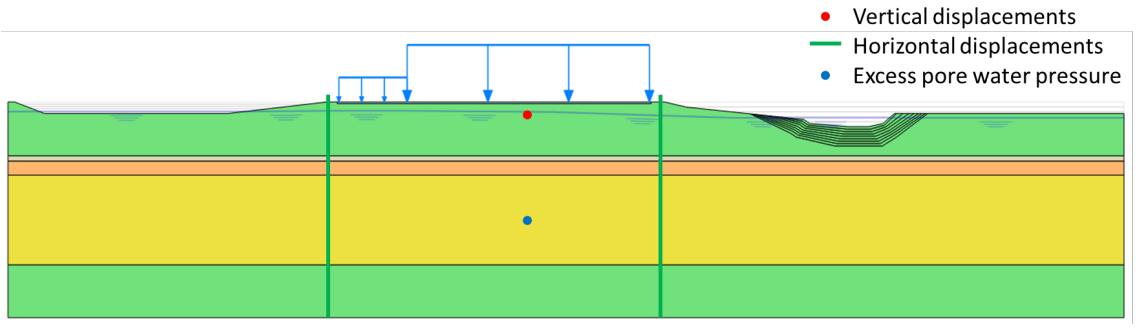

Figure E.5: Post-processing locations for section E.

F

Vertical displacements with time

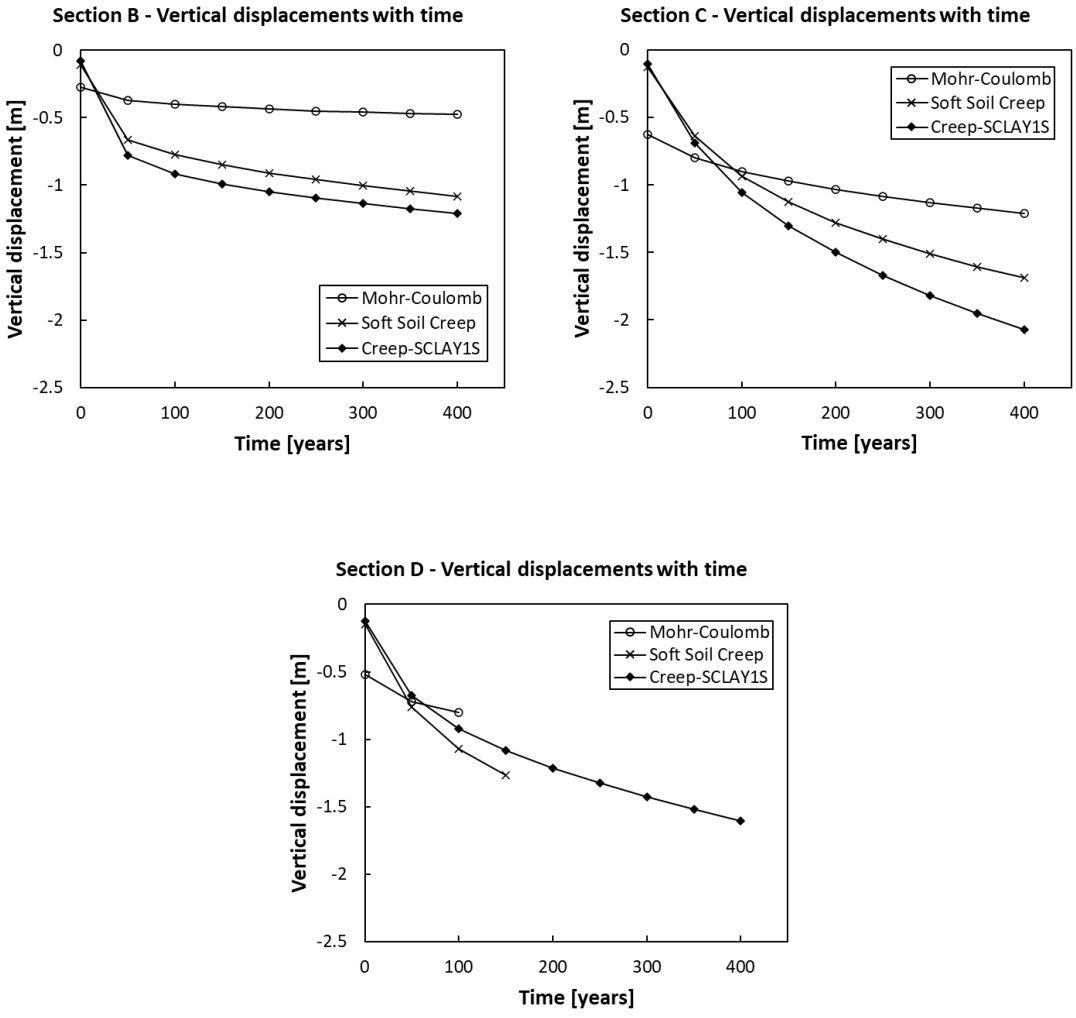

Figure F.1: Vertical displacement development over time for sections B, C, and D using different constitutive models.

G

Excess pore water pressure dissipation with time

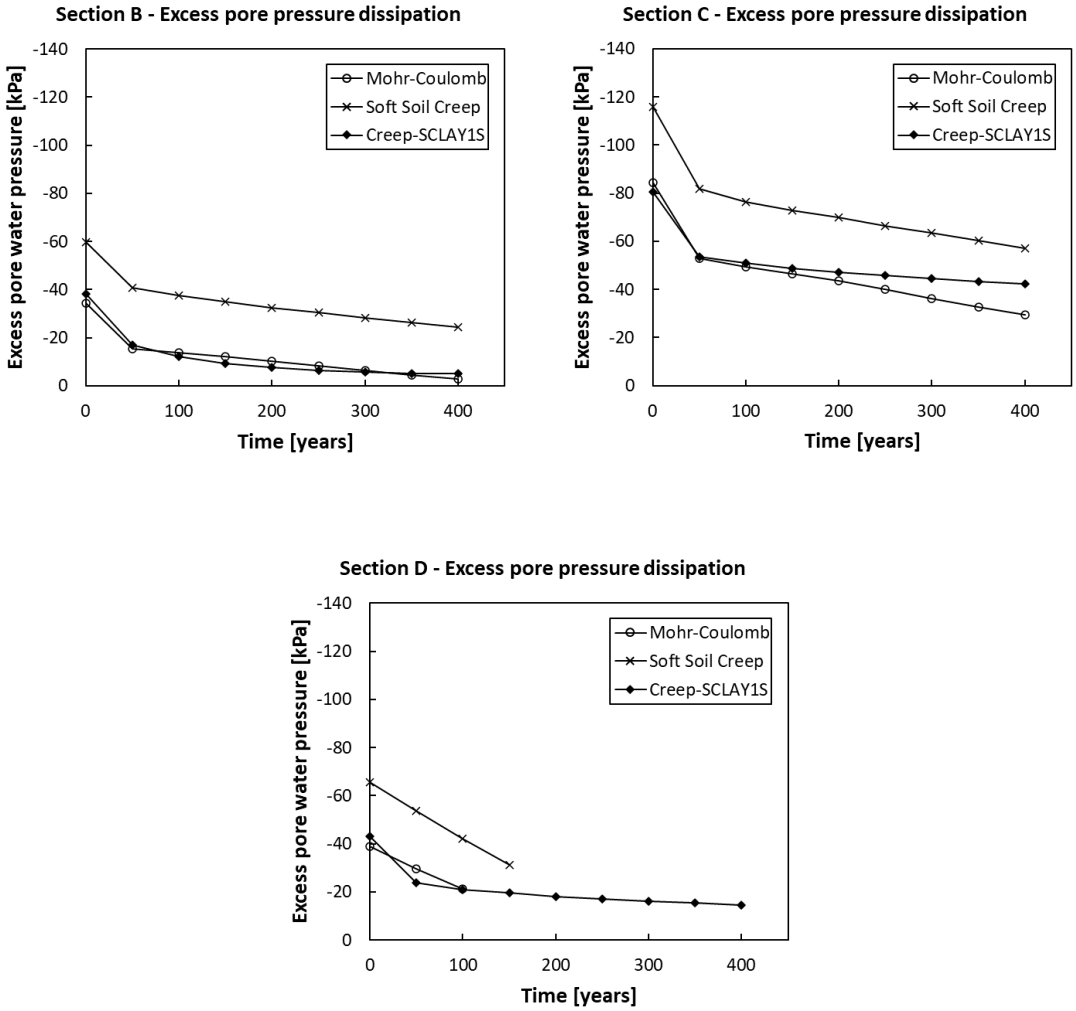

Figure G.1: Excess pore water pressure dissipation over time for sections B, C, and D using different constitutive models.

H

Horizontal displacement profiles

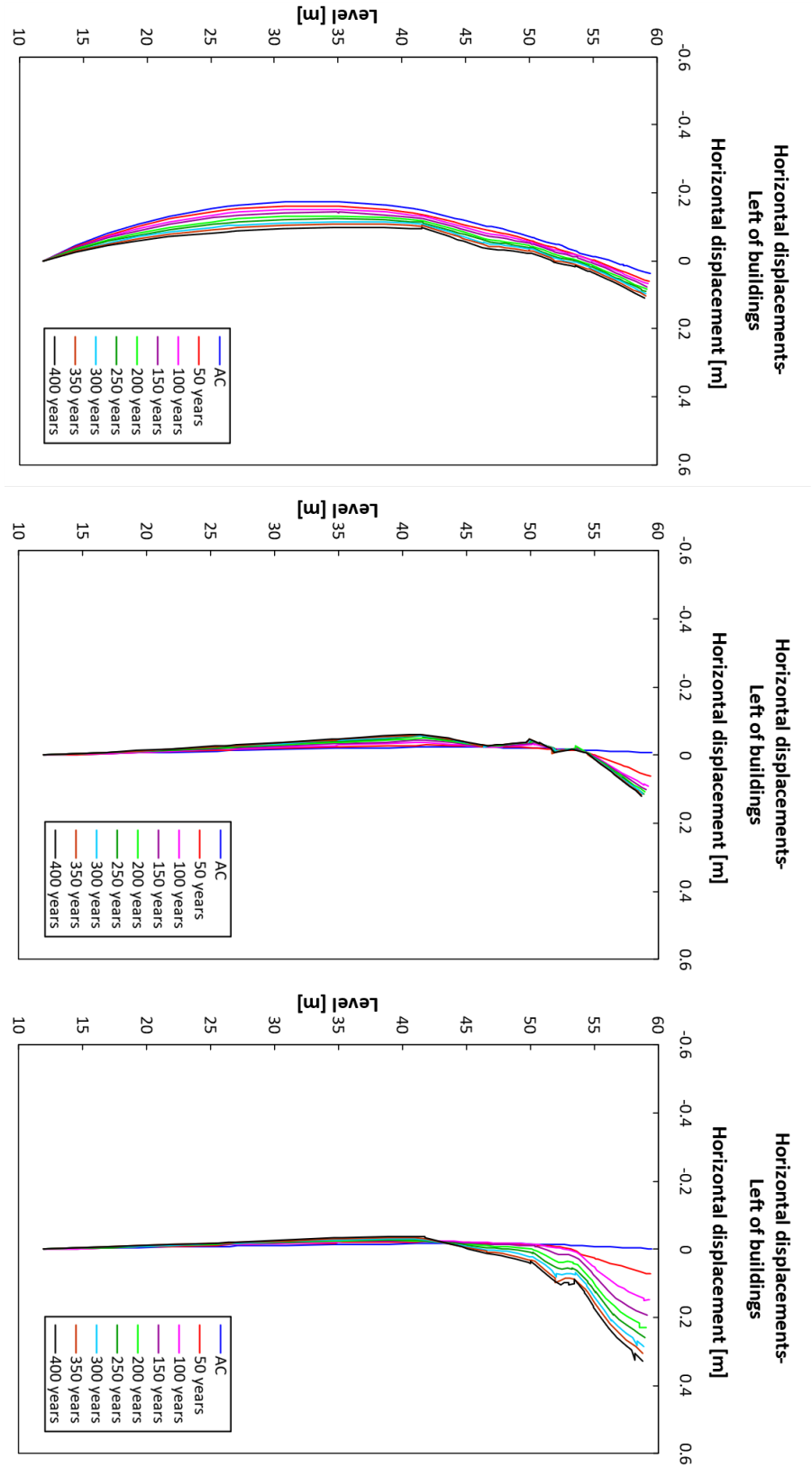

(a) Mohr-Coulomb

(b) Soft Soil Creep

(c) Creep-SCLAY1S

Figure H.1: Section A horizontal displacements in the left cross section with the different constitutive models.

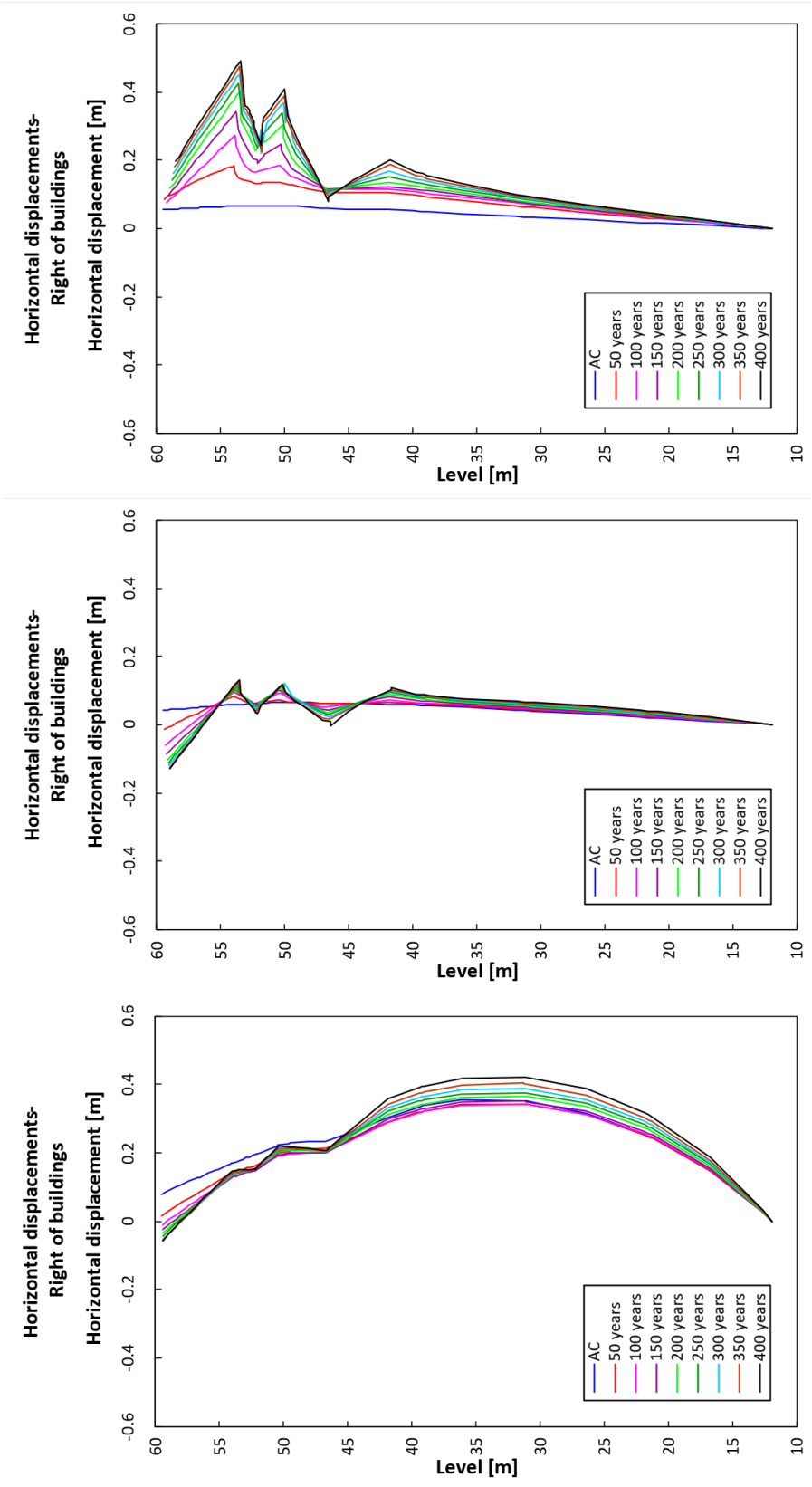

(a) Mohr-Coulomb (b) Soft Soil Creep (c) Creep-SCLAY1S

Figure H.2: Section A horizontal displacements in the right cross section with the different constitutive models.

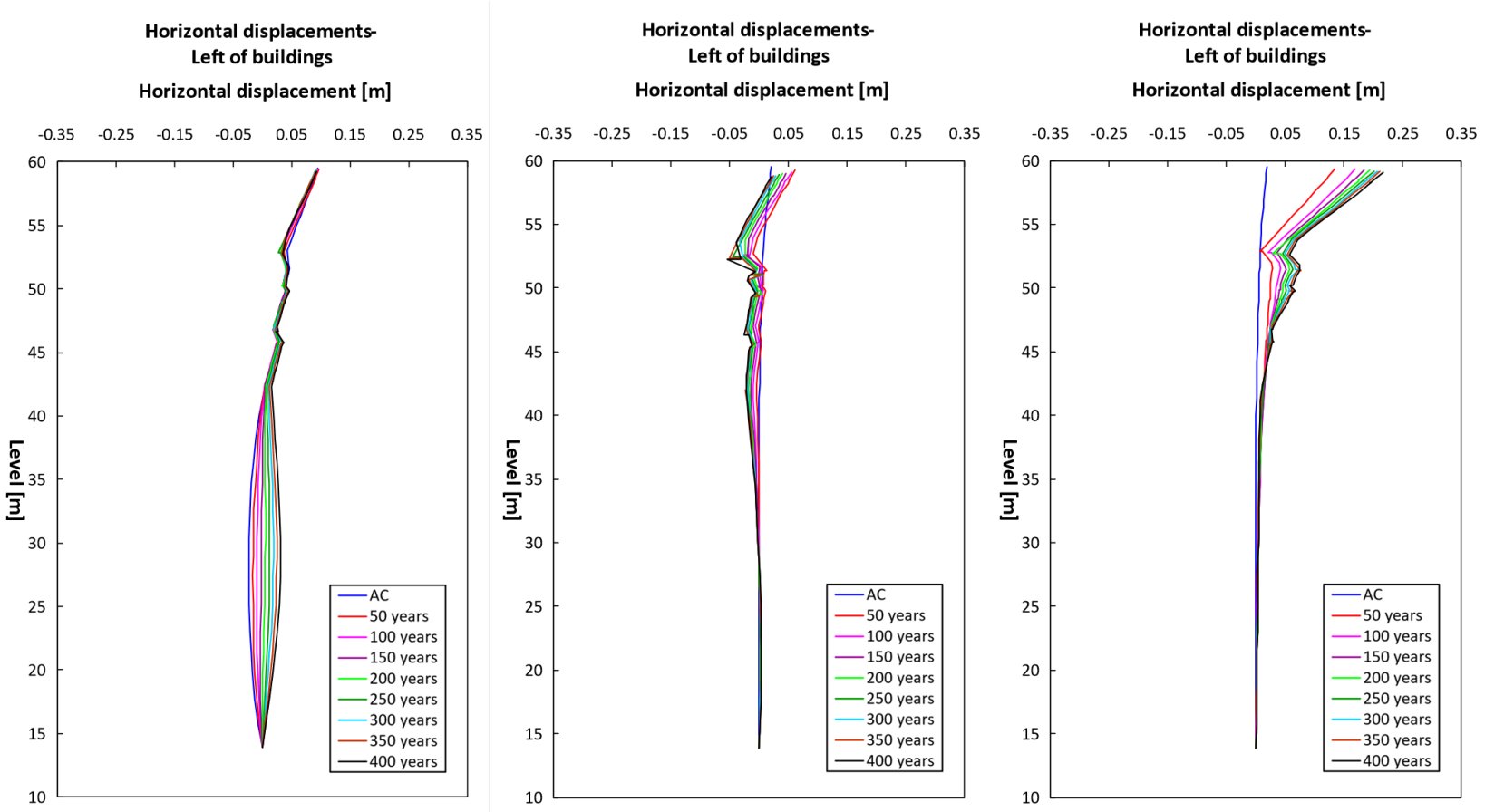

(a) Mohr-Coulomb (b) Soft Soil Creep (c) Creep-SCLAY1S

Figure H.3: Section B horizontal displacements in the left cross section with the different constitutive models.

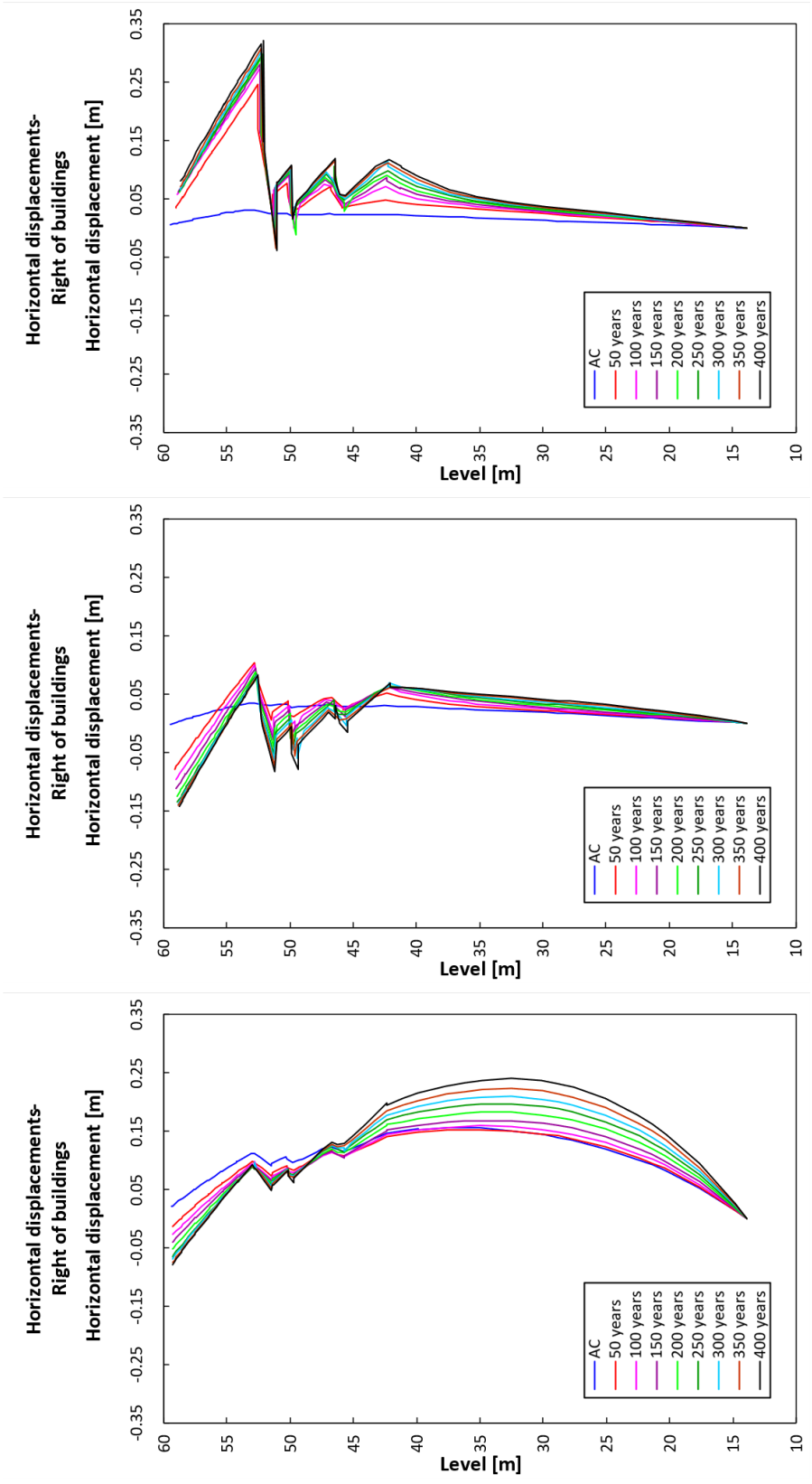

(a) Mohr-Coulomb (b) Soft Soil Creep (c) Creep-SCLAY1S

Figure H.4: Section B horizontal displacements in the right cross section with the different constitutive models.

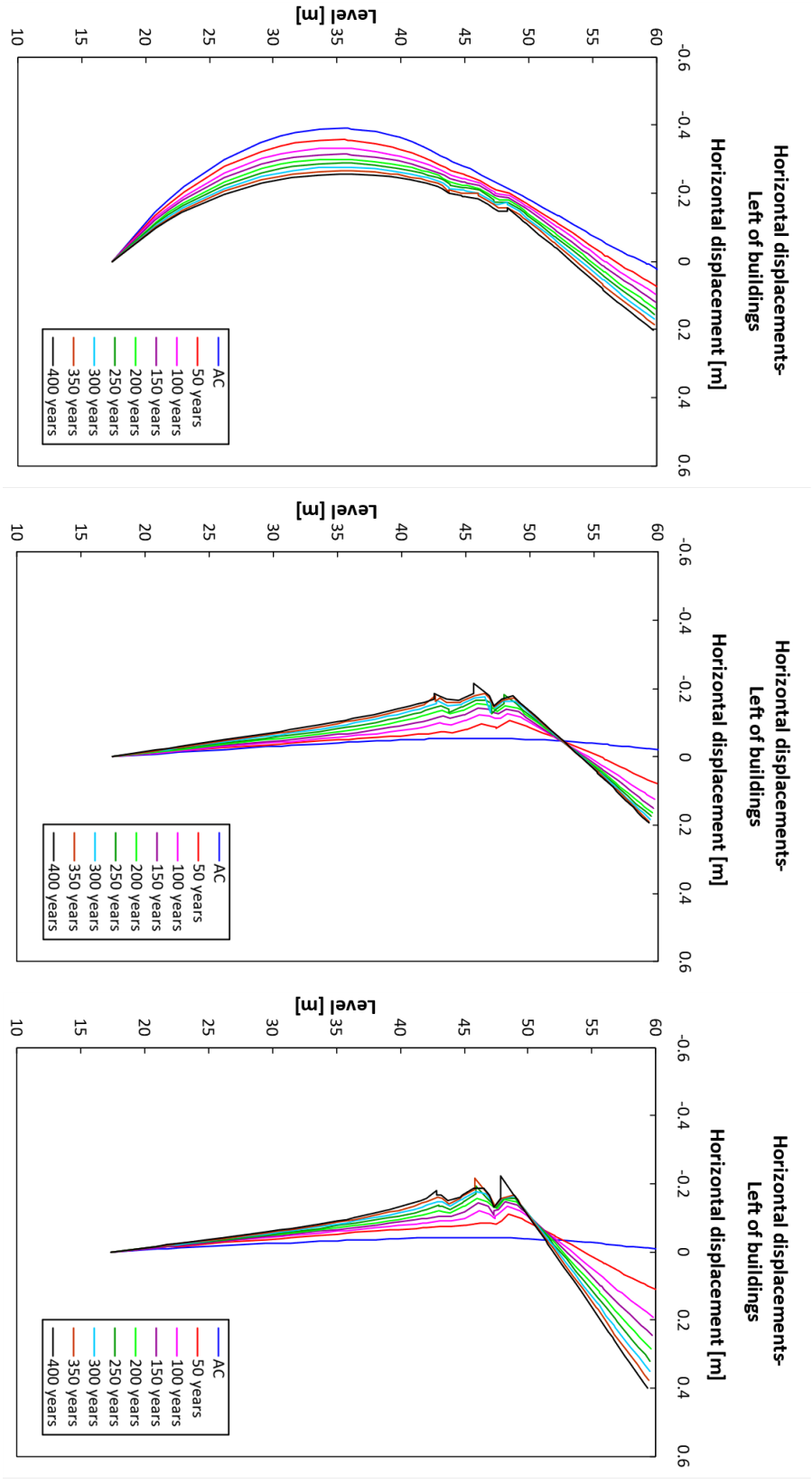

(a) Mohr-Coulomb

(b) Soft Soil Creep

(c) Creep-SCLAY1S

Figure H.5: Section C horizontal displacements in the left cross section with the different constitutive models.

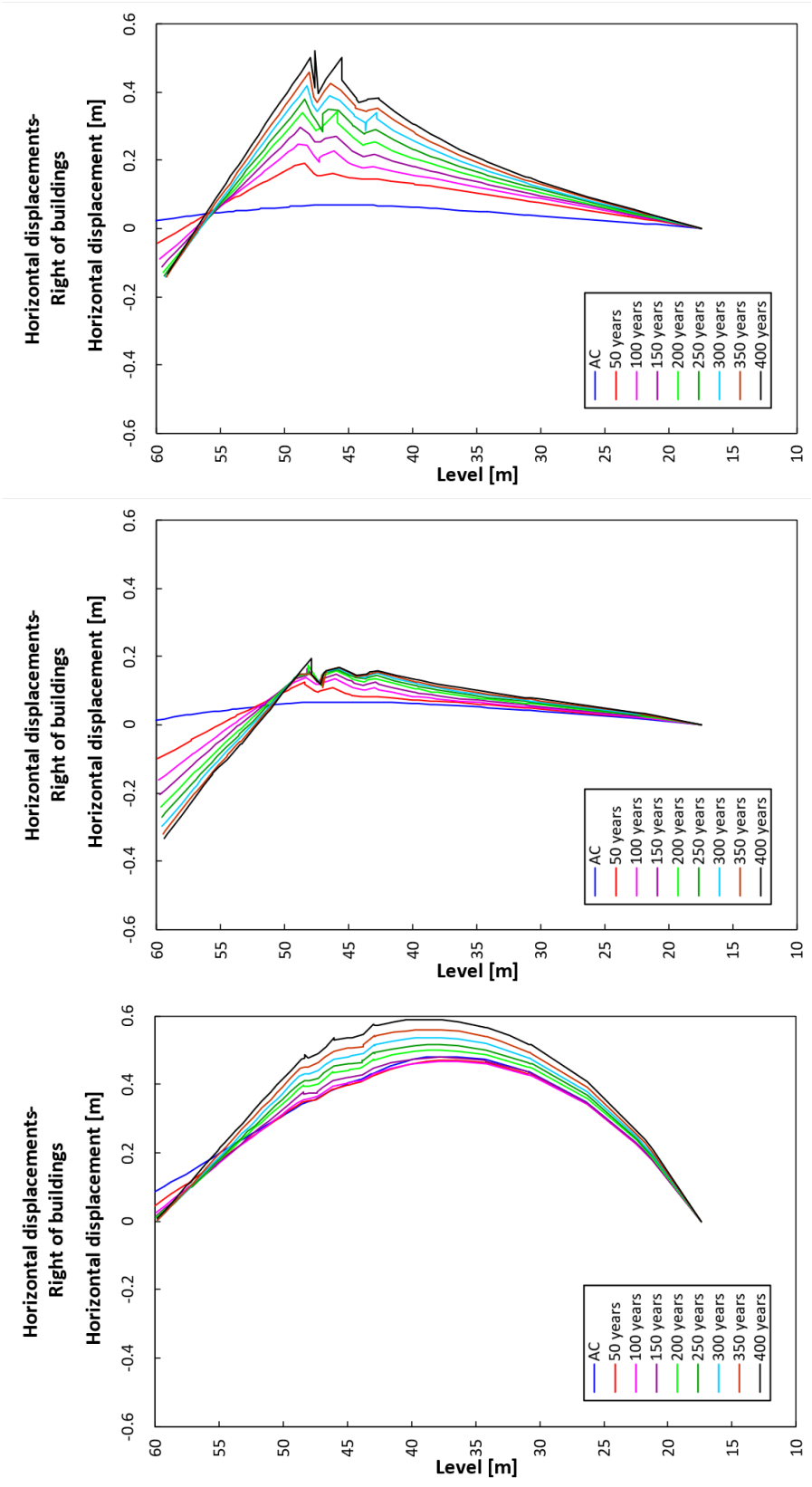

(a) Mohr-Coulomb (b) Soft Soil Creep (c) Creep-SCLAY1S

Figure H.6: Section C horizontal displacements in the right cross section with the different constitutive models.

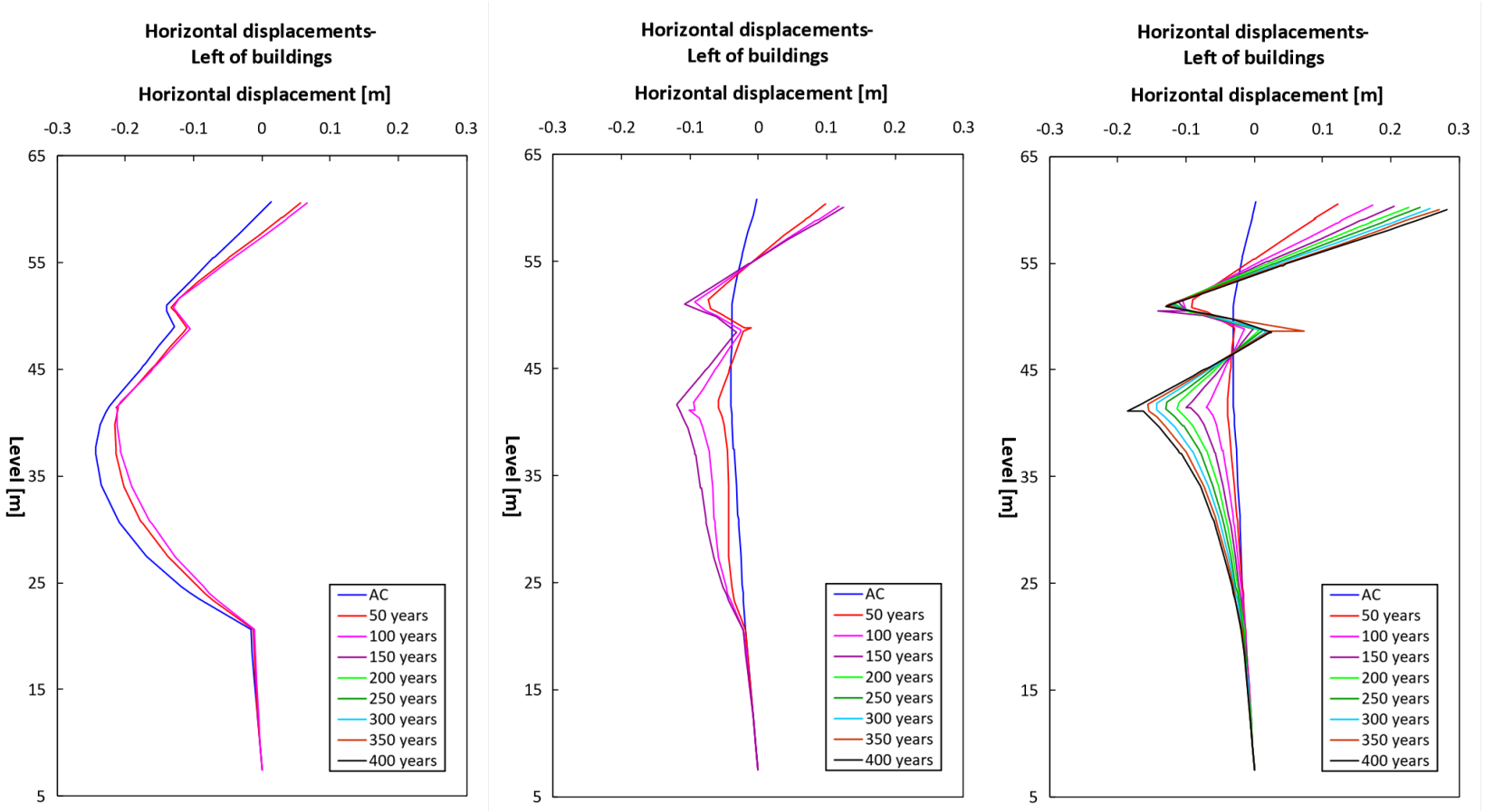

(a) Mohr-Coulomb (b) Soft Soil Creep (c) Creep-SCLAY1S

Figure H.7: Section D horizontal displacements in the left cross section with the different constitutive models.

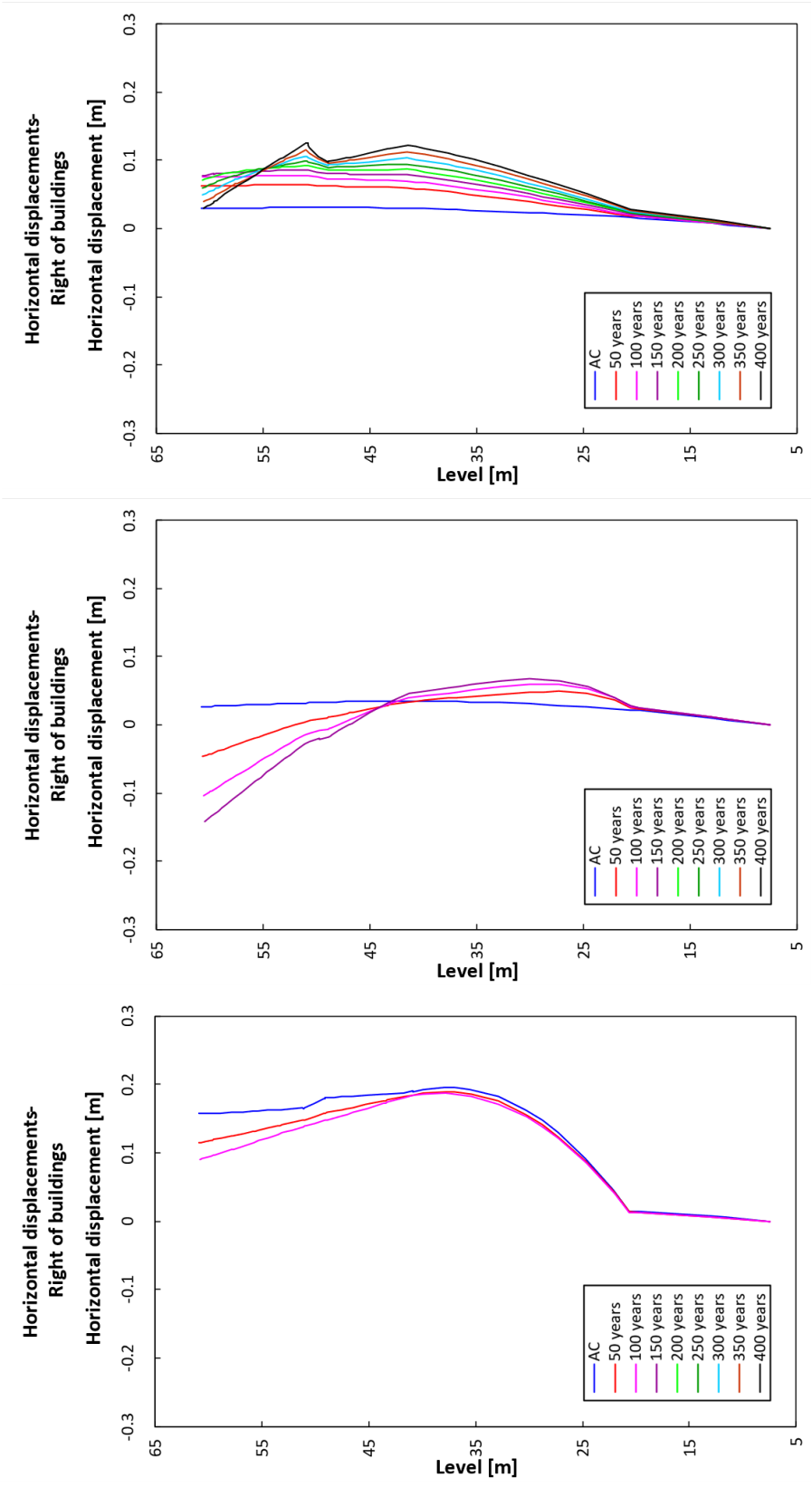

(a) Mohr-Coulomb (b) Soft Soil Creep (c) Creep-SCLAY1S

Figure H.8: Section D horizontal displacements in the right cross section with the different constitutive models.

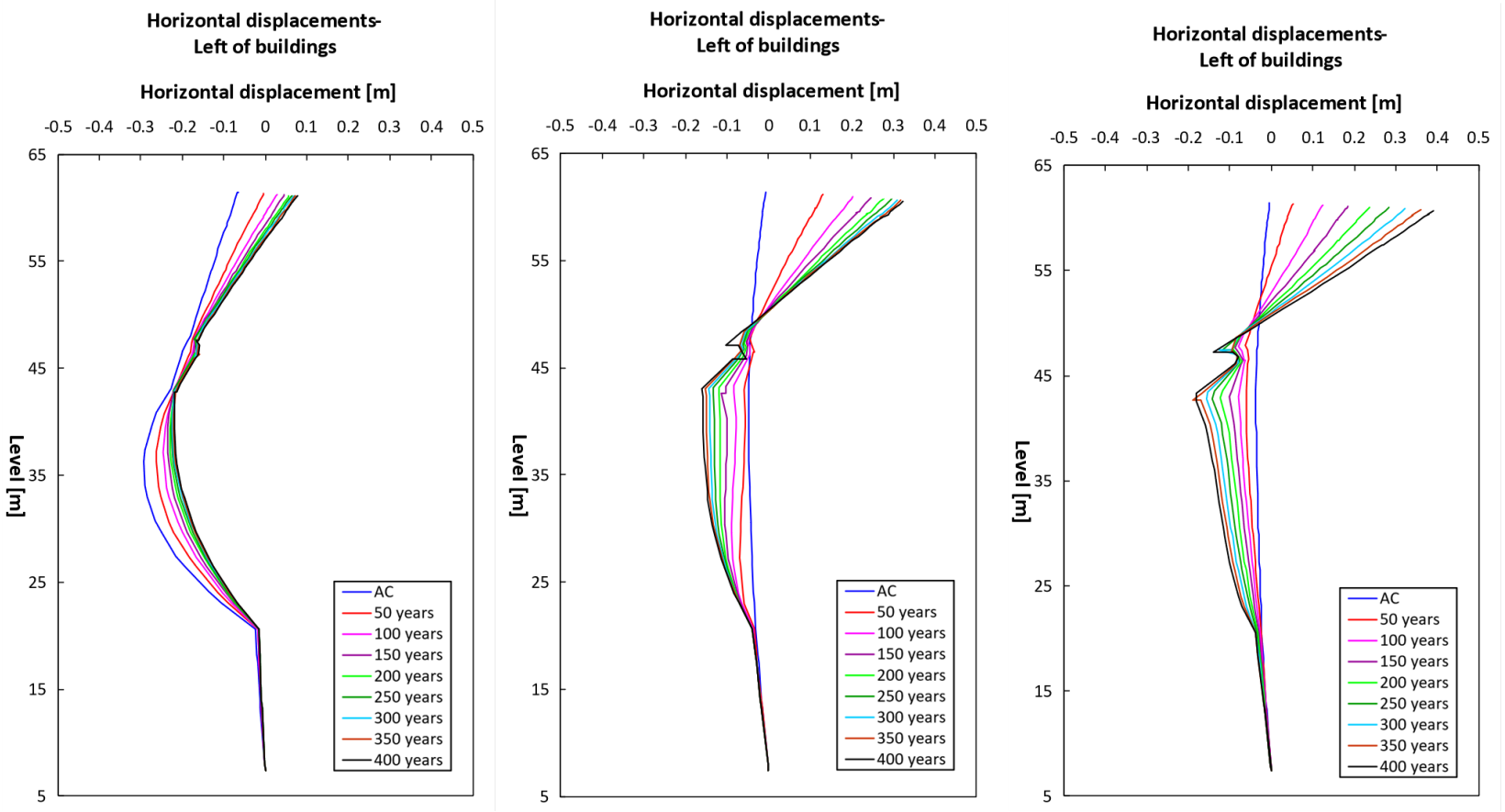

(a) Mohr-Coulomb (b) Soft Soil Creep (c) Creep-SCLAY1S

Figure H.9: Section E horizontal displacements in the left cross section with the different constitutive models.

I

Change in displacements due to erosion

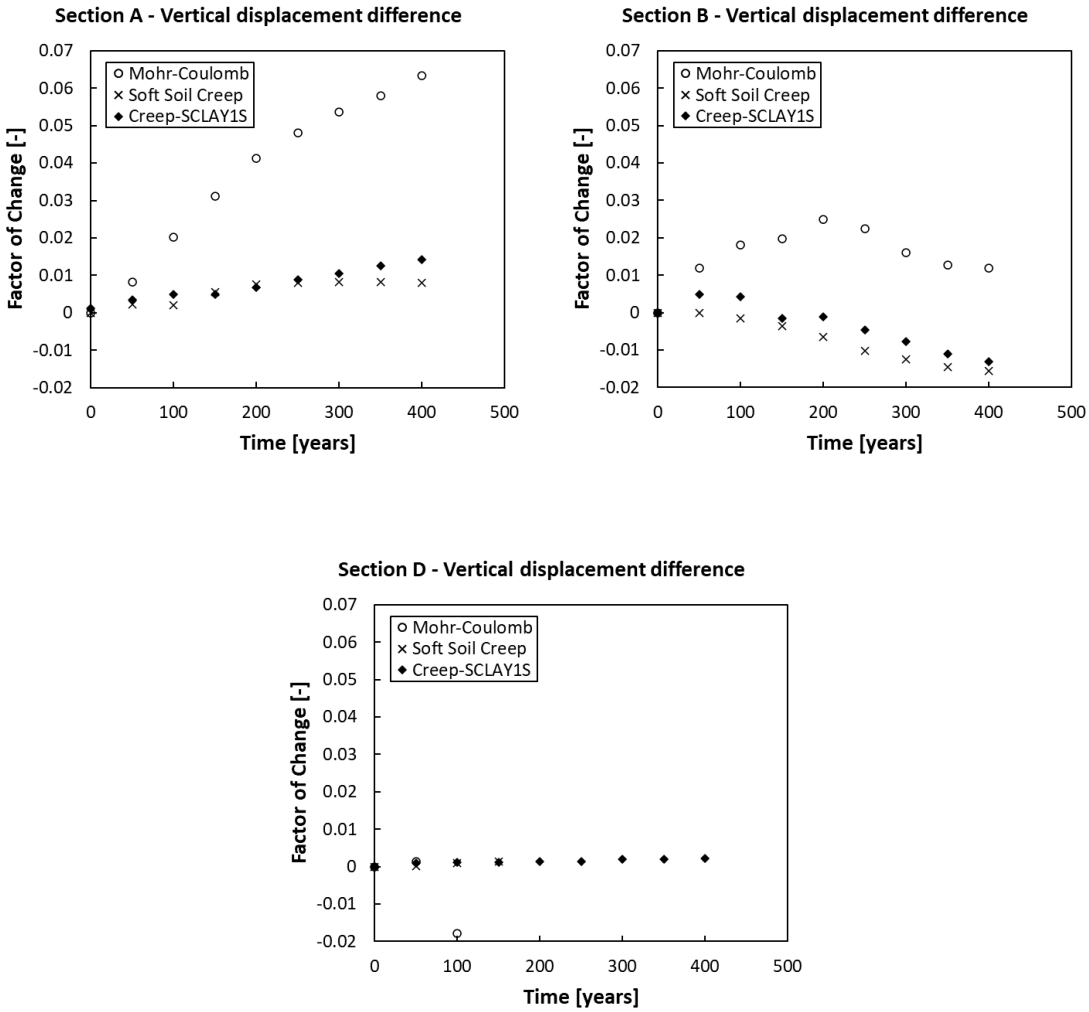

Figure I.1: Change in vertical displacements in sections A, B, and D as a result of modelling erosion.

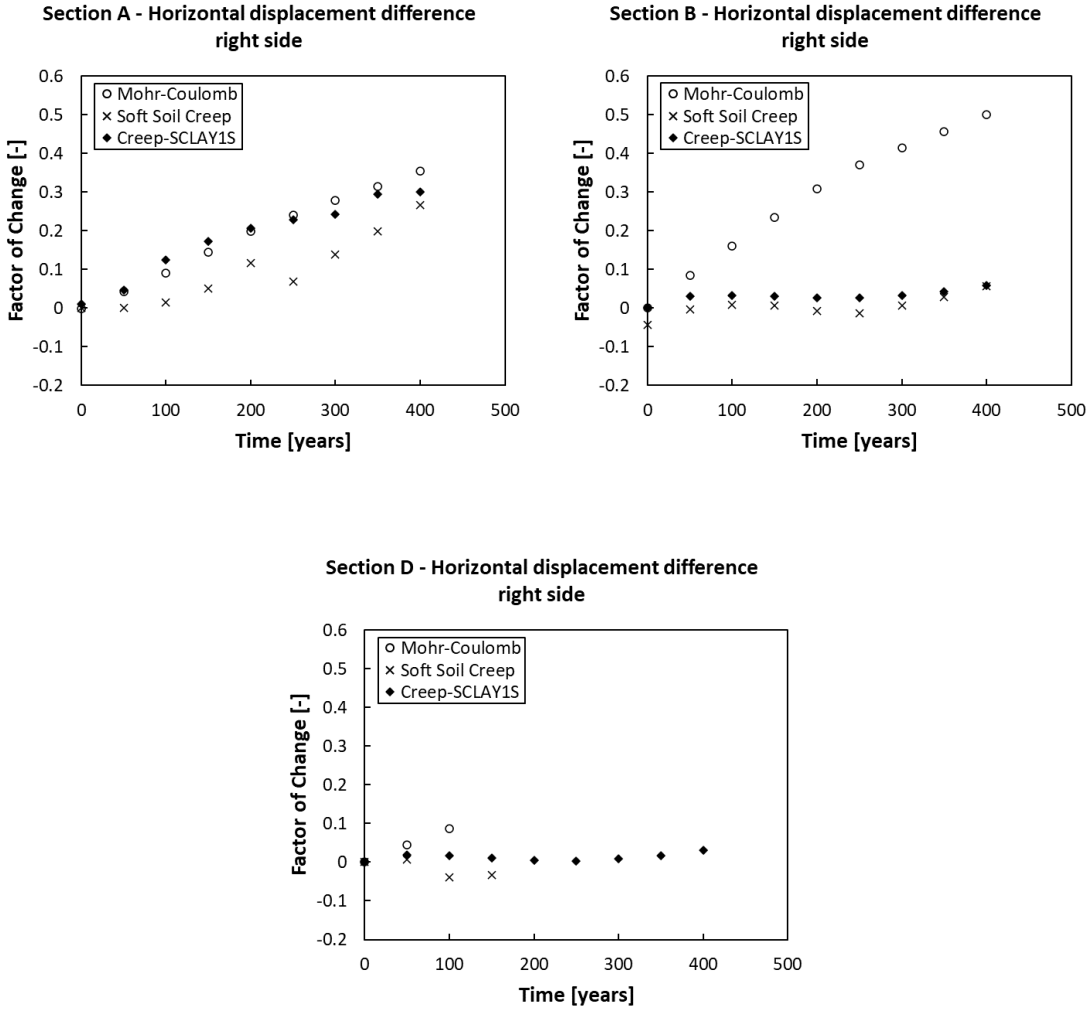

Figure I.2: Change in horizontal displacements in sections A, B, and D as a result of modelling erosion.

J

Development of incremental deviatoric strains with time

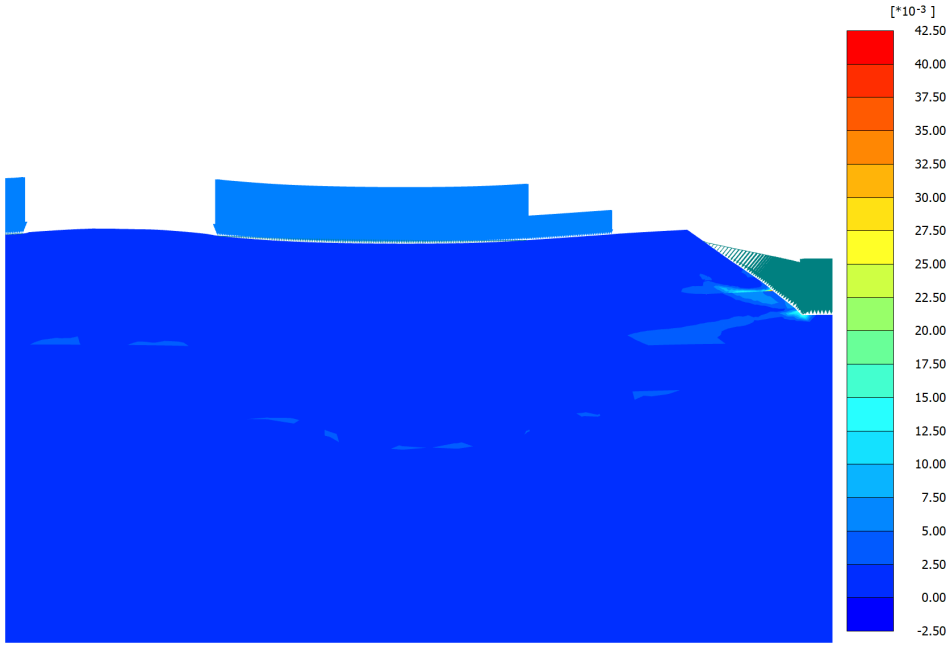

Figure J.1: Section profile showing the locations of the developing incremental deviatoric strains after 400 years using the Creep-SCLAY1S model in section A.

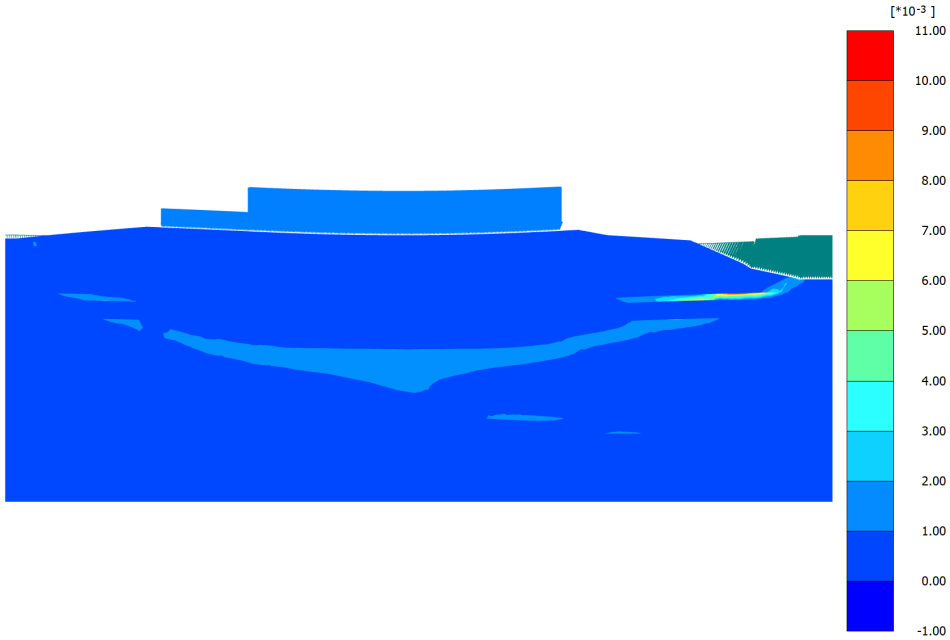

Figure J.2: Section profile showing the locations of the developing incremental deviatoric strains after 400 years using the Creep-SCLAY1S model in section E.

K

Effect on utilities

See Figures K.1-K.3 for the locations of the pipes in sections B, C, and E. These were used as post-processing locations when deriving the calculated displacements over time around these pipes, which can be seen in Figures K.4-K.9.

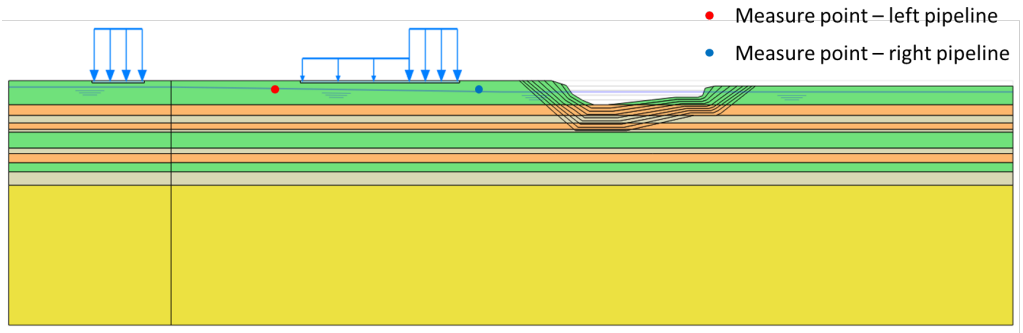

Figure K.1: Location of the pipelines in section B.

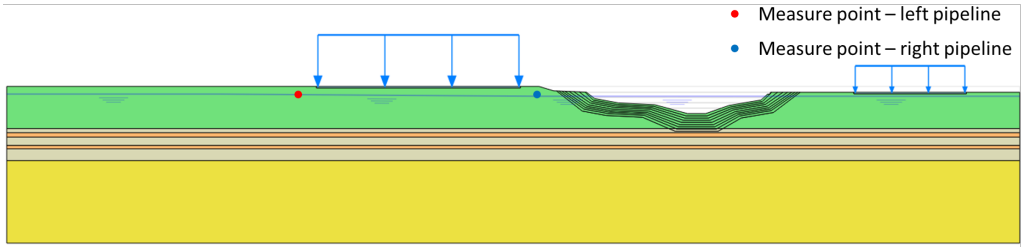

Figure K.2: Location of the pipelines in section C.

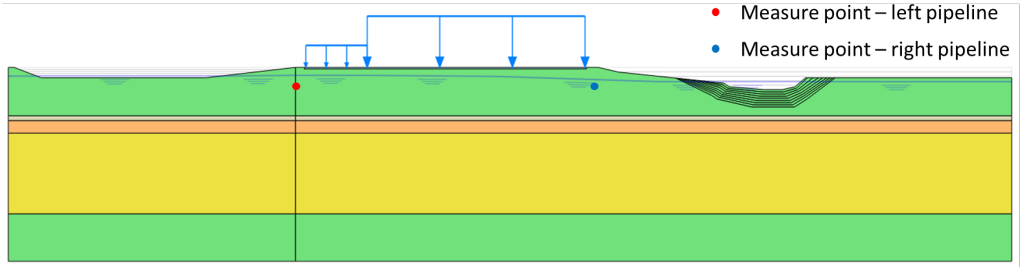

Figure K.3: Location of the pipelines in section E.

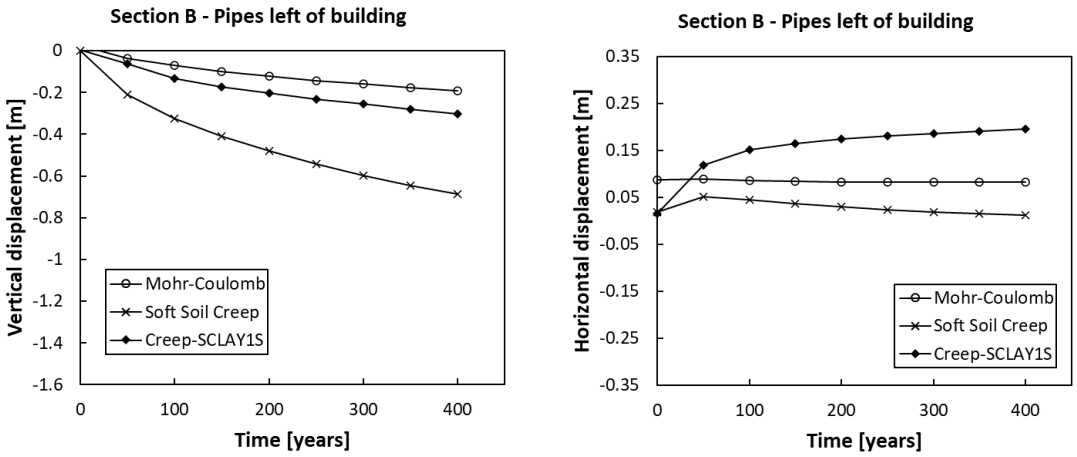

Figure K.4: Horizontal and vertical displacement over time around the pipes to the left of the building in section B.

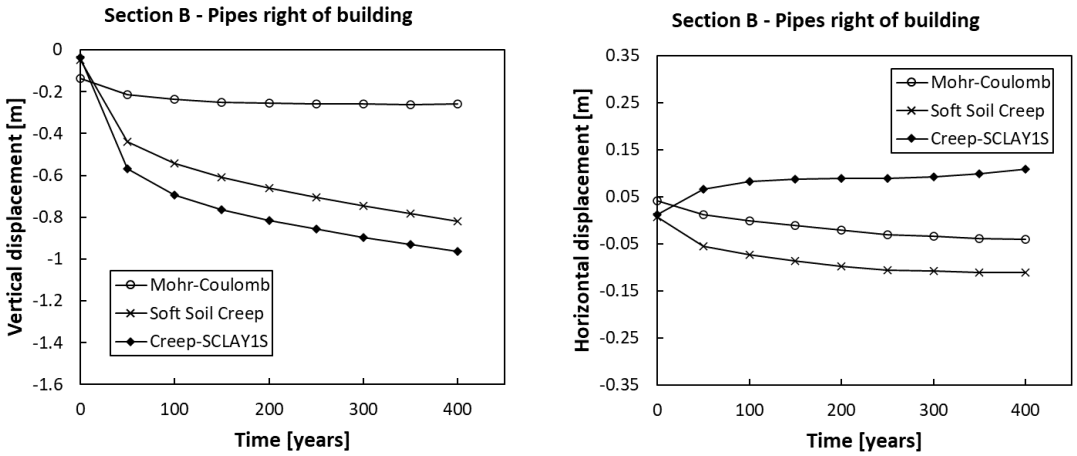

Figure K.5: Horizontal and vertical displacement over time around the pipes to the right of the building in section B.

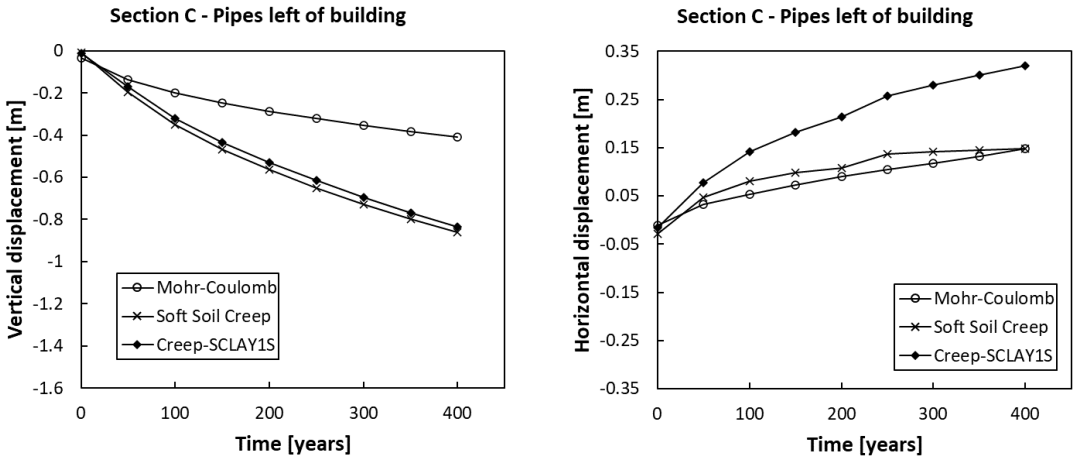

Figure K.6: Horizontal and vertical displacement over time around the pipes to the left of the basin in section C.

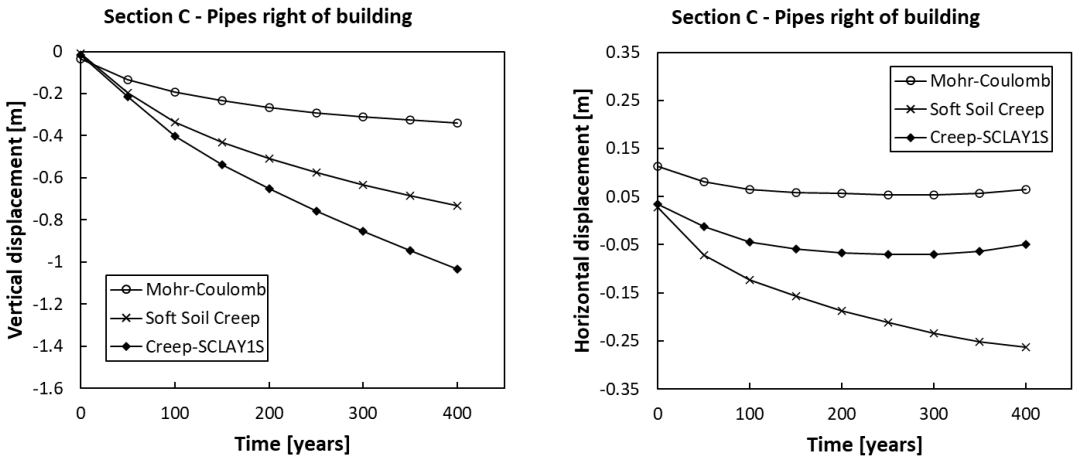

Figure K.7: Horizontal and vertical displacement over time around the pipes to the right of the basin in section C.

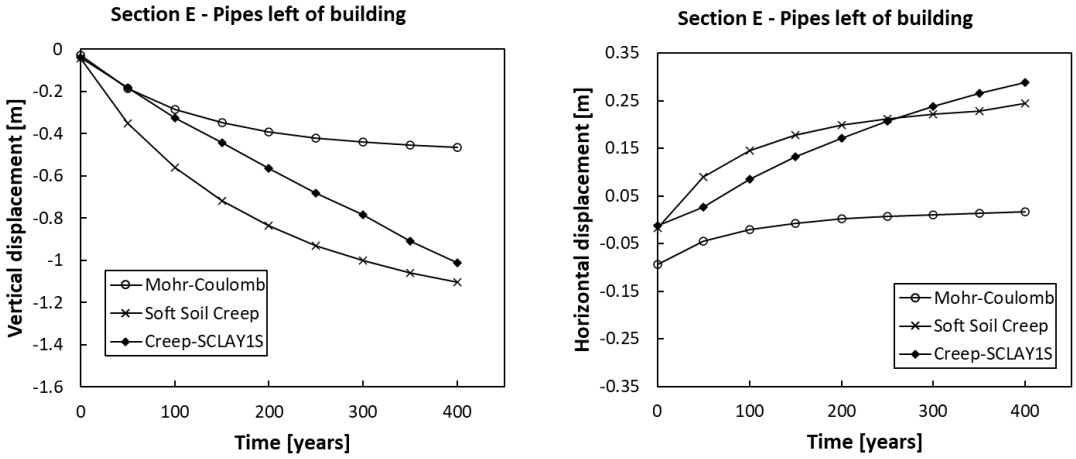

Figure K.8: Horizontal and vertical displacement over time around the pipes to the left of the buildings in section E.

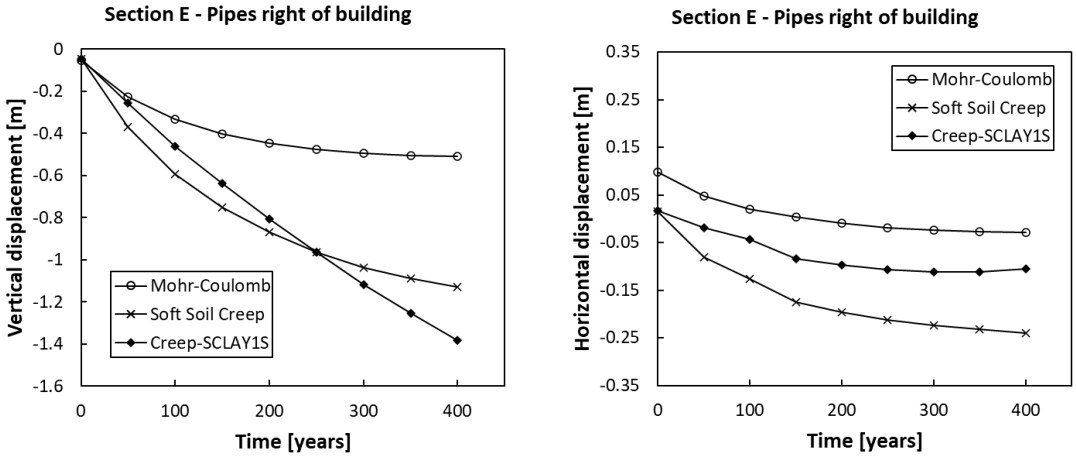

Figure K.9: Horizontal and vertical displacement over time around the pipes to the right of the buildings in section E.

DEPARTMENT OF ARCHITECTURE AND CIVIL ENGINEERING
CHALMERS UNIVERSITY OF TECHNOLOGY
Gothenburg, Sweden
www.chalmers.se

CHALMERS
UNIVERSITY OF TECHNOLOGY